Quaternary Science Reviews 147 (2016) 406–421

Contents lists available at ScienceDirect

Quaternary Science Reviews

journal homepage: www.elsevier.com/locate/quascirev

Late Quaternary vegetation and lake system dynamics in north-eastern Siberia: Implications for seasonal climate variability

B.K. Biskaborn [a, *], D.A. Subetto [b, c, d], L.A. Savelieva [e], P.S. Vakhrameeva [e, f], A. Hansche [a], U. Herzschuh [a, g], J. Klemm [a], L. Heinecke [a], L.A. Pestryakova [h], H. Meyer [a], G. Kuhn [i], B. Diekmann [a, g]

[a] Alfred Wegener Institute Helmholtz Centre for Polar and Marine Research, Potsdam, Germany
[b] Northern Water Problems Institute, Karelian Research Centre of Russian Academy of Sciences, Petrozavodsk, Russia
[c] Herzen State Pedagogical University of Russia, St. Petersburg, Russia
[d] Kazan (Volga) Federal University, Kazan, Russia
[e] St. Petersburg State University, St. Petersburg, Russia
[f] Arctic and Antarctic Research Institute, St. Petersburg, Russia
[g] University of Potsdam, Germany
[h] North-Eastern Federal University of Yakutsk, Russia
[i] Alfred Wegener Institute Helmholtz Centre for Polar and Marine Research, Bremerhaven, Germany

ARTICLE INFO

Article history:
Received 17 April 2015
Received in revised form
27 July 2015
Accepted 6 August 2015
Available online 3 September 2015

Keywords:
Diatoms
Pollen
Summer and winter temperature
Holocene Thermal Maximum
Aquatic and terrestrial ecosystems
Lake-ice cover

ABSTRACT

Although the climate development over the Holocene in the Northern Hemisphere is well known, palaeolimnological climate reconstructions reveal spatiotemporal variability in northern Eurasia. Here we present a multi-proxy study from north-eastern Siberia combining sediment geochemistry, and diatom and pollen data from lake-sediment cores covering the last 38,000 cal. years. Our results show major changes in pyrite content and fragilarioid diatom species distributions, indicating prolonged seasonal lake-ice cover between ~13,500 and ~8900 cal. years BP and possibly during the 8200 cal. years BP cold event. A pollen-based climate reconstruction generated a mean July temperature of 17.8 °C during the Holocene Thermal Maximum (HTM) between ~8900 and ~4500 cal. years BP. Naviculoid diatoms appear in the late Holocene indicating a shortening of the seasonal ice cover that continues today. Our results reveal a strong correlation between the applied terrestrial and aquatic indicators and natural seasonal climate dynamics in the Holocene. Planktonic diatoms show a strong response to changes in the lake ecosystem due to recent climate warming in the Anthropocene.

We assess other palaeolimnological studies to infer the spatiotemporal pattern of the HTM and affirm that the timing of its onset, a difference of up to 3000 years from north to south, can be well explained by climatic teleconnections. The westerlies brought cold air to this part of Siberia until the Laurentide ice-sheet vanished 7000 years ago. The apparent delayed ending of the HTM in the central Siberian record can be ascribed to the exceedance of ecological thresholds trailing behind increases in winter temperatures and decreases in contrast in insolation between seasons during the mid to late Holocene as well as lacking differentiation between summer and winter trends in paleolimnological reconstructions.

1. Introduction

The Arctic is experiencing unprecedented warming (PAGES 2k consortium, 2013). During the Anthropocene warming has greatly exceeded the global average temperature increase, due to a mechanism called “Arctic amplification” (IPCC, 2013; Miller et al., 2010a). In northern Asia, the effect of recent climate warming is most intense in eastern Siberia (Jones et al., 1999). There, biosphere responses to climate change include not only shifts in geographical distribution but also extinction of species unable to adapt fast enough to new environmental conditions (MacDonald et al., 2008). Subrecent short-term climate changes are also associated with societal reactions, such as the disappearance of northern or alpine

Supplementary data are available at http://dx.doi.org/10.1594/PANGAEA.848906.

* Corresponding author.
E-mail address: boris.biskaborn@awi.de (B.K. Biskaborn).

http://dx.doi.org/10.1016/j.quascirev.2015.08.014
0277-3791/

human populations during historical cooling events (Grove, 2004; Kotlayakov et al., 2014; Wanner et al., 2011) or to the present threat to northern communities caused by permafrost degradation, increasing forest fires and other extreme events (AMAP, 2012). However, the climate at northern latitudes since the late-glacial period has been spatially variable and complex (Kaufman et al., 2004; Miller et al., 2010b) and modern Arctic landscapes are affected by recent climate change with varying severity (IPCC, 2014). A precise understanding of the spatial and temporal variability of the environmental history of the Arctic is thus necessary for the sustainment of favourable ecological and economic conditions and the better prediction of future scenarios.

Past climate change at a supra-millennial scale was driven by insolation anomalies, which resulted from cyclic changes to orbital parameters known as Milankovich cycles, whereas natural and anthropogenic controlled land-surface characteristics and greenhouse-gas emissions are the drivers of sub-millennial scale changes (Jones et al., 2009; Miller et al., 2010b; Wanner et al., 2011). Profound research on Holocene climate variability inferred from lake sediments has been reviewed and reported during the last decade (e.g. Kaufman et al., 2004; Kaufman et al., 2009; Miller et al., 2010b; Sundqvist et al., 2014; Wanner et al., 2008, 2011). Investigations of sediment cores from lakes in north-eastern Siberia are known from the Lena Delta area (Andreev et al., 2004; Biskaborn et al., 2013a; Laing et al., 1999; MacDonald et al., 2004; Pisaric et al., 2001; Porinchu and Cwynar, 2002) and its hinterland (Biskaborn et al., 2013b, 2012; Herzschuh et al., 2013; Müller et al., 2009, 2010; Popp et al., 2006). Synthesising these reports shows that climate development, especially in the early and mid Holocene, varied at local to regional scales and the so-called Holocene Thermal Maximum (HTM) is strikingly different across space and time. Temperature reconstructions during the mid to late Holocene in the Northern Hemisphere are, however, often based on summer proxies and biased due to insufficient differentiation between summer and winter temperatures (Meyer et al., 2015). In the literature cited above, climate reconstructions for Siberia are mainly based on terrestrial and aquatic bioindicators, but to understand better the role of winter and summer temperatures in the sedimentary and fossil record palaeolimnological studies should integrate the tight and complex hydrologic coupling between terrestrial and aquatic environments in boreal lake ecosystems (Engstrom et al., 2000).

The timing of climate changes, as reported for the western and eastern Arctic, is spatially asynchronous and knowledge gaps in millennial-scale climate variability still exist, particularly for large areas in north-eastern Siberia. In this paper we present a multi-proxy study combining sediment geochemistry, and diatom and pollen data from a lake-sediment archive in the lower Lena River area in north-eastern Siberia. Our objectives are (i) to reconstruct the depositional environment and to constrain the timing of major palaeoenvironmental changes during the last ~38,000 years at Lake Kyutyunda, (ii) to assess the influence of summer and winter climate conditions on terrestrial and aquatic indicators, and (iii) to reveal spatiotemporal patterns of major Holocene climate events by comparing our results with other palaeolimnological reconstructions from north-eastern Siberia.

2. Regional setting

Lake Kyutyunda (N 69°38′, E 123°38′, 66 m a.s.l.) is located 320 km south of the Lena Delta in the Molodo River valley and 45 km west of the Lena River in Yakutia, north-eastern Siberia, Russia (Fig. 1). The lake extends 2.2 km from north to south and 3 km from east to west, with a surface area of about 4.9 km^2. The deepest part in the centre of the smooth lake basin is ca. 3.5 m. The estimated average water depth is ca. 2.5 m.

Lake Kyutyunda is on the central Siberian Plateau near the transition to the Verkhoyansk mountain region. The study area is situated in the northern taiga zone, approximately 120 km south of the present treeline. The vegetation is characterised by an open *Larix* forest intermixed with shrub-tundra. According to the geological map of Yakutia (Prokopiev et al., 1999) the bedrock of the catchment mainly consists of Middle Jurassic sandstone and unconsolidated sands (Kystatymskaya suite). The western and northwestern shore of the lake is underlain by Pliocene and Lower and Upper Pleistocene sands and gravels (Prokopiev et al., 1999). These deposits are identified as alluvium – the remains of flood-plain terraces of the Molodo River (Geological map of the USSR, Vysotsky (1970)). Clear evidence of a former river bed identified from LANDSAT imagery (Fig. 1) and confirmed by field observations, as well as the lake's close proximity to the Molodo River, indicate a fluvial-erosion thermokarst lake (Pestryakova et al., 2012). Soils in this area are predominantly north-taiga gley and gleyic undifferentiated soils (Agricultural Atlas of the Yakut ASSR, Matveev (1989)). We observed dune sands west of the lake and different peat generations at the southern and western shoreline. Permafrost in this region reaches down to a maximum of 700 m (Kondratieva, 1989). During fieldwork in summer 2010, the active layer was about 50 cm deep.

The recent climate in northern Siberia is strongly influenced by the track of the westerlies. During winter, the region lies roughly between the 'Siberian High' and the Laptev Sea coast (MacDonald et al., 2000).

The area is characterised by a pronounced continental climate. Present-day mean July and January temperatures for the Lena hinterland are at the coast 8 °C and −36 °C, respectively with a mean annual temperature of about −14 °C; maximum July and minimum January temperatures are 30 °C and −60 °C (Shahgedanova, 2002). Southwards, at the town of Yakutsk, with increasingly continental climate mean July and January temperatures are 19.5 °C and −38.6 °C, respectively, with a mean annual temperature of about −8.8 °C. However, modern temperatures based on MODIS satellite imagery and the interpolated WORLDCLIM data at the study location indicate mean July temperatures between 13 °C and 15 °C (Duguay et al., 2012; Hijmans et al., 2005). Annual precipitation in the Lena Delta region is mainly represented by summer rainfall of about 200 mm (Boike et al., 2008). Direct precipitation, run-off, and one small inflow coming from a smaller lake 4.5 km east feed the lake. One small outflow drains from the south-western side of the lake towards the Molodo River, 3.4 km to the west. During summer it is likely that the lake is permanently mixed (polymictic).

3. Materials and methods

3.1. Field work

Sediment cores were taken during a helicopter expedition to Lake Kyutyunda between August 17 and September 3, 2010. Lake basin bathymetry was measured with a portable Depthmate SM-5 Echo Sounder to locate the appropriate coring site at a deep and undisturbed part of the basin. Water samples for hydrochemical analyses of the water column were collected from the core site before and after sediment coring, to avoid biased data due to suspension load. Immediately after collection, the water samples were analysed using a WTW Multilab 340i for pH, conductivity, and oxygen values. A sub-sample of the original water was passed through a 0.45 μm filter, and then stored and transported in 60-ml Nalgene polyethylene bottles for subsequent anion and cation analyses. Cation samples were acidified with HNO_3 in the field.

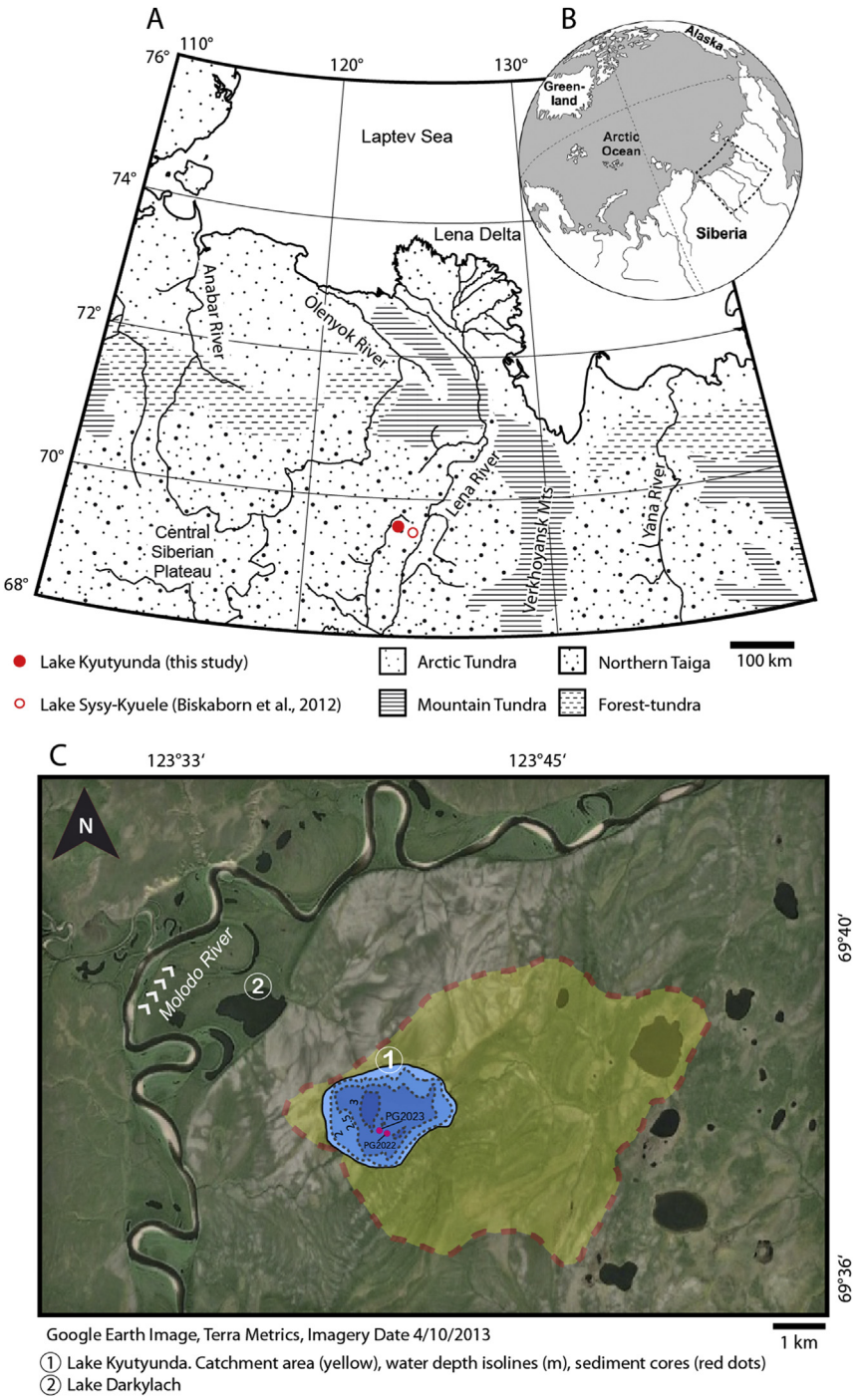

Fig. 1. A. Location of Lake Kyutyunda in north-eastern Siberia (Sakha Republic, Yakutia), Russia. Vegetation zones from Tishkov (2002). B. Study area on a globe. C. Landsat satellite image showing water bodies, vegetation cover, and flow directions of the Molodo River. Water depth and position of the sediment cores PG2023 and PG2022 are marked in the lake. Catchment is indicated by red-dashed line. (For interpretation of the references to colour in this figure legend, the reader is referred to the web version of this article.)

The sediment cores were retrieved from an anchored platform using a Russian peat corer (core PG2022) and a UWITEC piston coring system (core PG2023). The distance between the two coring sites is ca. 65 m; coordinates are given in the caption of Table 1. Core PG2022 was retrieved as a series of six half cores (1 m length, 7.5 cm diameter) with an 80 cm overlap in the upper section and 20 cm overlaps in the lower sections. After immediate sedimentological inspection of the core on the platform, the core sections were stored in PVC half tubes. Core PG2023 was retrieved as a series of 3 m sections in transparent PVC coring tubes (6 cm diameter) with 1 m overlaps. Cores were split into 1 m sections for transportation in insulated boxes.

3.2. Laboratory analyses

3.2.1. Sediment core treatment

Core PG2023 and water samples from Lake Kyutyunda were analysed in the laboratories of the Alfred Wegener Institute,

Table 1
Radiocarbon dates and age modelling results. Calibrated years BP, modelled years BP, and 2σ-ranges were calculated using the IntCal09 (Reimer et al., 2009) calibration curve in OxCal 4.1 (Ramsey, 2009). Methods: TOC – bulk organic carbon (SOL plus RES). RES – insoluble fraction (alkali residual, humins). SOL – alkali soluble fraction (humic fraction). Core site PG2022: N 69° 37.711′ E 123° 38.888′. Core site PG2023: N 69° 37.702′ E 123° 38.987′.

Core ID, depth (cm)	Composite depth (cm)	Lab-ID	14C age BP, error	Cal. yrs median	2 sigma cal.	Modelled yrs median	2 sigma modelled	Sample type
PG2022-1_0-0.5	0.25	Poz-50551	1010 ± 50	–	–	–	–	TOC, 0.6 mgC
PG2022-1_0-0.5	0.25	Poz-50553	1140 ± 40	–	–	–	–	SOL, 0.3 mgC
PG2022-1_0-0.5	0.25	Poz-50554	930 ± 40	–	–	–	–	RES, 0.5 mgC
PG2023-2_50.5-51	72	Poz-49481	2405 ± 35	2427	2683–2347	2438	2691–2347	RES
PG2023-2_71.5-72	93	Poz-49472	3585 ± 30	3888	3978–3829	3839	3925–3718	RES
PG2023-2_188-188.5	210.5	Poz-49471	5900 ± 40	6720	6842–6638	6710	6799–6635	RES
PG2023-3_79-79.5	305	Poz-49470	8000 ± 50	8867	9011–8655	8818	8994–8651	RES
PG2023-3_187-187.5	413	Poz-49474	9420 ± 50	10,651	10,777–10,509	11,040	11,095–10,947	RES
PG2023-3_244-244.5	470	Poz-49483	10,620 ± 60	12,570	12,675–12,421	12,670	12,901–12,551	RES
PG2023-4_78.5-79	493	Poz-49482	13,360 ± 100	16,435	16,847–15,618	16,543	16,859–15,990	RES
PG2023-5_25-26	560.5	Poz-50560	27,820 ± 300	32,020	32,888–31,391	31,247	31,498–31,046	RES, 0.5 mgC
PG2023-4_231-232	645.5	Poz-50555	33,500 ± 500	–	–	–	–	TOC
PG2023-4_231-232	645.5	Poz-50557	29,180 ± 350	33,847	34,645–32,995	34,644	35,158–34,268	RES, 0.5 mgC
PG2023-4_231-232	645.5	Poz-50556	33,900 ± 700	–	–	–	–	SOL, 0.4 mgC
PG2023-5_162.5-163	698	Poz-49484	33,770 ± 350	38,633	39,649–37,371	37,959	38,885–37,252	RES

Helmholtz Centre for Polar and Marine Research (AWI) in Potsdam and Bremerhaven (Germany). The PVC liners and sediments were cut into two equal halves along the long axis. The 'work half' was subsampled and the 'archive half' was used for core description and non-destructive X-ray fluorescence scanning. Analyses on core PG2022 were conducted in the Russian–German Otto Schmidt Laboratory, Arctic and Antarctic Research Institute, St. Petersburg (Russia). In both cores, sample resolution was designed according to the scale of expected palaeoenvironmental changes aimed to detect.

3.2.2. Dating

For dating, eleven bulk sediment samples were taken from core PG2023 at intervals of about 75 cm (Table 1) and sent to Poznan Radiocarbon Laboratory. Accelerator Mass Spectrometer (AMS) radiocarbon dates were calculated based on insoluble humin fractions (RES), alkali-soluble humic acids fractions (SOL), and total organic carbon (TOC) of dispersed organic carbon from bulk sediment material. Since the SOL fraction resulted in slightly older ages than the RES fraction, we opted to use the dates of the latter methods as there was likely less bias from contamination of the sediment by vertically migrating dissolved radiocarbon.

Radiocarbon dates were calibrated using the IntCal09 calibration curve (Reimer et al., 2009) in OxCal 4.1 (Ramsey, 2009) and used to generate an age–depth model (Fig. 2). Time scales are based on linear interpolation between two neighbouring median values of modelled years BP.

Additional ^{210}Pb dating of the upper 20 cm of core PG2022 was carried out in the Radium Institute, St. Petersburg, Russia. Mean sedimentation rate was calculated from the upper- and lower-most values of the measured ^{210}Pb activity between 0 and 14 cm.

3.2.3. Hydrochemistry

From 5 depth profile water samples and 2 surface water samples, pH and oxygen were measured using a WTW Multilab 340i in the field. Other hydrochemical analyses were undertaken in the laboratories at AWI Potsdam in 2012. Due to a delay in the delivery of the samples from Russia to Germany, alkalinity was not measured. Anions were analysed using a Dionex DX 320 Ion Chromatographer; cations were determined using a Perkin-Elmer Optima 8300DV Perkin-Elmer – Optical Emission Spectrometer (ICP-OES).

3.2.4. X-ray fluorescence and diffractometry

The elemental composition of core PG2023 was semi-quantitatively analysed by X-ray fluorescence using the Avaatech XRF core scanner at AWI Bremerhaven with an Rh X-ray tube at 1.8 mA, 10 s count time, and 30 kV (without filter). Spatial logging resolution (slit) was 5 mm (downcore, 12 mm wide) resulting in 1422 downcore measurements. The mean error of the XRF measurements, expressed as chi square (χ^2) modelled to measured peak intensity curve fitting for the relevant elements, was 0.6 for Zr; 0.8 for Sr; 0.7 for Rb; and 0.8 for Br.

The mineralogical composition of 104 freeze-dried and milled samples from core PG2023 were analysed by X-ray diffractometry (XRD) using a Philips PW1820 goniometer at AWI Bremerhaven (40 kV, 40 mA, from 3 to 100°, step-rate 0.05°, Co kα radiation). XRD data were processed using MacDiff 4.0.7 (freeware developed by R. Petschick in 1999). To avoid the influence of opal and organic material, peak area intensities of minerals were plotted versus the sum of the peak area intensities (total intensity) of all minerals.

3.2.5. Carbon and nitrogen analyses

In core PG2023, carbon and nitrogen were measured from 116 samples at 2 cm intervals in the uppermost 20 cm, followed by 5 cm intervals until 5 m core depth and 25 cm intervals until the core's bottom at 7 m. Total carbon (TC) and total nitrogen (TN) of freeze-dried and milled samples were quantified by heating the material in small tin capsules using a Vario EL III carbon–nitrogen–sulphur (CNS) analyser. Total organic carbon (TOC) was measured with a Vario MAX C analyser. The per cent by weight of TOC and TN were used to calculate the TOC/TN_{atomic} ratio following Meyers and Teranes (2002). The stable carbon isotope composition of the total organic carbon fraction was measured in 56 samples taken at intervals of 4 cm in the uppermost 20 cm, followed by 10 cm intervals until 5 m, and at 50 cm intervals until 7 m depth in core PG2023. $\delta^{13}C$ was measured using a Finnigan Delta-S mass spectrometer after inorganic carbon removal by hydrochloric acid treatment. Results are expressed as $\delta^{13}C$ values relative to the PDB standard in parts per thousand (‰) with an error of ±0.15%.

From core PG2022 we extracted 291 subsamples at intervals of 2 cm for loss-on-ignition analysis (LOI, % of dry weight) using a SNOL 7,2/1100 (AB "Umega", Lithuania) muffle furnace. LOI was measured by burning the samples at 550 °C for 4 h, cooling them down in a desiccator, and measuring the weight of the ash residuals. The procedure was repeated until a constant weight was measured. Mass difference between the dry sediment and the ash residue was used as a proxy for the sedimentary organic matter. Thus we could correlate the two sediment cores and transfer the age–depth model of PG2023 to PG2022.

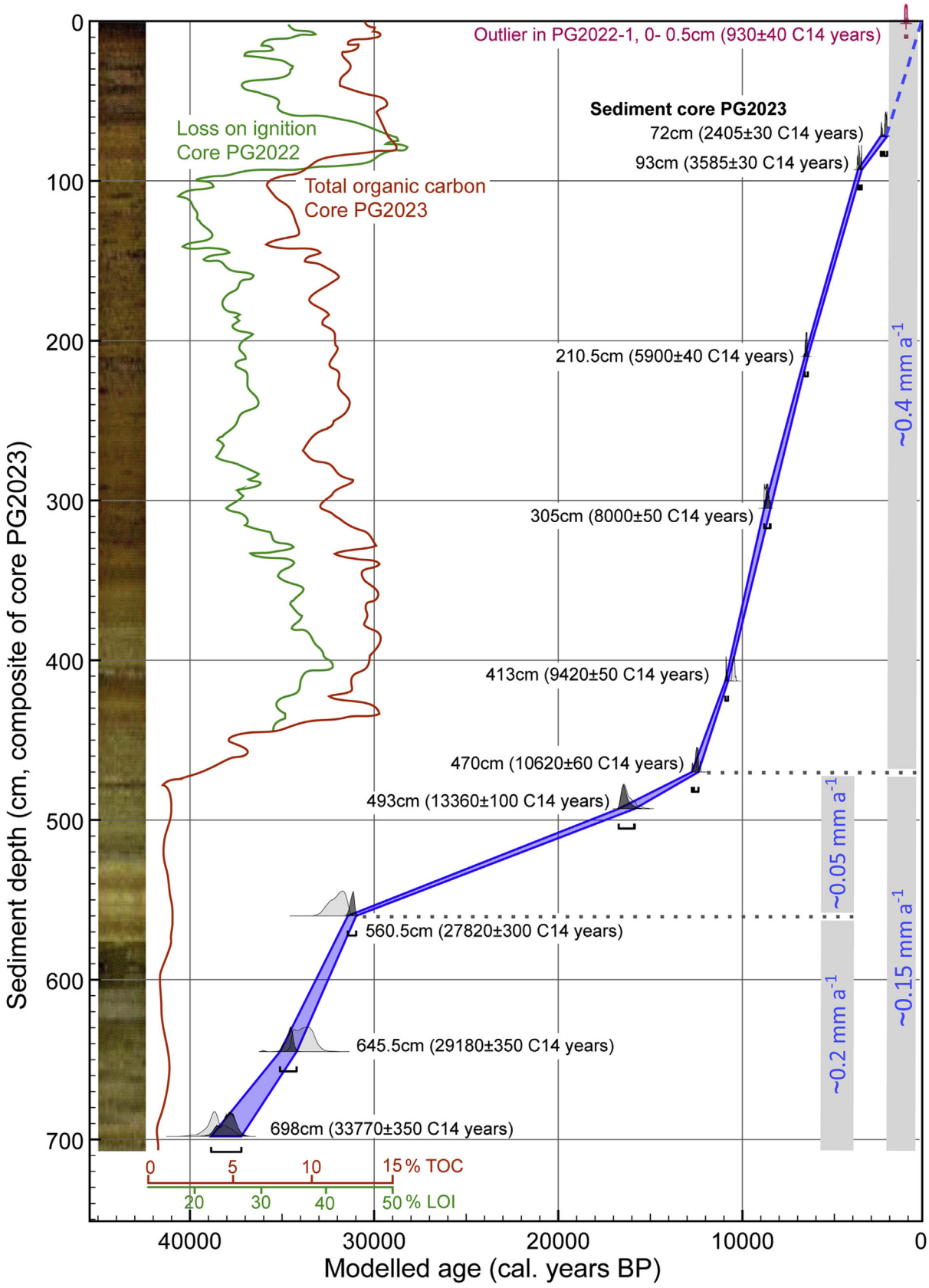

Fig. 2. Age–depth model. Calibration and modelling was performed using OxCal 4.1 (Ramsey, 2009) with the IntCal09 data set (Reimer et al., 2009). The modelled age is plotted against depth with linear interpolation between the modelled 2σ-ranges (95.4% probability). The dashed blue line is the linear interpolation from the youngest modelled age to the sediment surface (~0 BP) from ^{210}Pb dating. Loss-on-ignition (green line) and total organic carbon (red line) were used for tuning the age–depth model of core PG2023 to core PG2022. (For interpretation of the references to colour in this figure legend, the reader is referred to the web version of this article.)

3.2.6. Diatoms

From core PG2023 a total of 34 samples at a 2–10 cm resolution from 0 to 1 m and at 20 cm intervals from 1 to 4.6 m was prepared for diatom analysis following the standard procedure described by Battarbee et al. (2001). 5×10^6 microspheres were added to each sample for later calculation of the diatom valve concentration (DVC). Diatom slides were prepared on a hot plate using Naphrax mounting medium. For the identification of diatoms to the lowest possible taxonomic level several keys were used, including Lange-Bertalot et al. (2011), Lange-Bertalot and Metzeltin (1996), Krammer and Lange-Bertalot (1986–1991) and Lange-Bertalot and Genkal (1999). Where possible, a minimum of 300–350 diatom valves were counted in each sample using a Zeiss AXIO Scope.A1 light microscope with a Plan-Apochromat 100×/1.4 Oil Ph3 objective at 1000× magnification. In one sample at 4.6 m, only 46 valves were present; this sample is marked in the diagram (Fig. 6). Chrysophyte cysts were enumerated for calculating the chrysophyte cyst/diatom ratio (C/D) following Smol (1985). Where possible, identification of small diatom species was verified using a scanning electron microscope (SEM) at the GeoForschungsZentrum Potsdam.

The diatom stratigraphical succession, was zoned using constrained incremental sum-of-squares cluster analysis (CONISS: Grimm, 1987). To mitigate the effect of highly abundant fragilarioid species, clustering was based on square-root transformed percentage data from all diatom taxa present. The broken-stick method (Bennett, 1996), based on the Bray–Curtis distance, was performed to assess the significance of created zones.

Diatom-inferred alkalinity values are expressed as concentrations of HCO_3^- ions. They were estimated using the quantitative transfer function developed by Herzschuh et al. (2013) based on weighted-averaging partial least-squares regression. A modern training dataset including diatom taxa and hydrochemical data from 201 lakes in Yakutia was used in the transfer function applied to the fossil diatom assemblages from Lake Kyutyunda. Validation of the model yields a root-mean square error of prediction (RMSEP) of 0.3log+1 mg L^{-1}.

3.2.7. Pollen

Pollen analysis was carried out at St. Petersburg State University. Pollen and spores were extracted from 30 samples from core PG2022 according to standard procedures, including treatment with HCL and NaOH and a heavy liquid separation (Berglund and Ralska-Jasiewiczowa, 1986), followed by preparation on glycerol mounts. At least 150 and at most 400 pollen grains of terrestrial plants were identified and counted in each sample using a stereomicroscope at 400× magnification. Taxonomic identifications followed Kupriyanova and Alyoshina (1972, 1978), Moore et al. (1991), Savelieva et al. (2013), and the modern pollen reference collection of St. Petersburg State University. Calculated pollen percentages refer to the total sum of terrestrial pollen. Additionally, green algae of *Pediastrum*, spores and redeposited pollen taxa (Tertiary spores and redeposited Quaternary pollen) were counted.

Detailed pollen analysis was based on the square-root transformed data of the terrestrial pollen, which were employed in the cluster analysis and the descriptive principal component analysis. A stratigraphically-constrained cluster analysis (CONISS) was based on the Bray–Curtis dissimilarity matrix and combined with the broken-stick model (see Diatoms section above). To reconstruct past summer temperature, a pollen-climate transfer function exclusively based on pollen spectra from 111 lake surface-sediments from northern Siberia was used; a detailed description is given in Klemm et al. (2016). The number of pollen taxa used was reduced to 24 pollen taxa to reduce taxonomic bias due to different palynologists counting the fossil and modern pollen. This reduction slightly decreases the performance of the calibration set for the modelled mean July temperature (T_{July} RMSEP 1.65 °C; maximum bias 4.23 °C). To test the final reconstructed T_{July}, the correlation between species optima and redundancy ordination axis scores was assessed against 999 reconstructions from random environmental data (Telford and Birks, 2011). The statistical pollen data analysis was performed in the R environment (R Core Team, 2012) using the analogue (Simpson et al., 2014), rioja (Juggins, 2014), and palaeoSig (Telford, 2015) packages. The pollen diagram was created in C2 version 1.7.6 (Juggins, 2007).

4. Results

4.1. Chronology

Calibration and modelling of the radiocarbon-dated samples in core PG2023 (Table 1) provide a stratigraphically consistent age–depth relationship (Fig. 2). Three fractions measured from the surface sample from the other core (PG2022, 0–0.5 cm) returned an age of about 1000 radiocarbon years BP, but ^{210}Pb dating analyses of this core (PG2022) confirmed that the surface sediments represent recent material. The ^{210}Pb analyses measured unsupported ^{210}Pb of 16.7 ± 3.9 Bq kg^{-1} at 13–14 cm depth increasing linearly to 163.0 ± 8.5 Bq kg^{-1} at 0–2 cm core depth. Based on this relationship, the mean sedimentation rate of the surface sediments in this part of the Kyutyunda basin was calculated to be 1.7 ± 0.2 mm y^{-1}. Accordingly, the overly old radiocarbon date from PG2022 was treated as an outlier. The carbon and mineral analyses recorded negligible amounts of carbonate in the sediment and processes other than a hard-water effect may have caused the overly old radiocarbon date of the surface sample, possibly contamination. In the uppermost 18 cm of core PG2023, TOC/TN_{atomic} values increase dramatically suggesting a major change in the mode of carbon accumulation affecting the carbon quality.

As the radiocarbon dates between the surface and 4.7 m core depth show a clear linear relationship trending towards zero years BP (AD 2010) at the surface, we have no reasons to doubt these dates. Radiocarbon ages below 4.9 m indicate less constant sedimentation rates in a non-lake sedimentological setting.

The age–depth model for core PG2023, which is based on ten radiocarbon dates and ^{210}Pb dating of the surface sediments from PG2022, spans the time interval between ca. 38,000 years BP and the present day. The main change in sedimentation rates from ~0.15 to ~0.4 mm a^{-1} is consistent with the lithological change separating the Pleistocene and the Holocene located at ~4.7 m core depth (Fig. 2). Very low sedimentation rates (0.05 mm a^{-1}) were calculated between 4.7 and 5.6 m, indicating a possible existence of one or more hiatuses in this core section.

To transfer the age–depth model between the sediment cores, PG2023 and PG2022 were correlated and the depth axis of PG2022 was rescaled using total organic carbon (TOC) and loss on ignition values (LOI). Tuning was performed using ANALYSERIES 2.0.8 (Paillard, 1996). The linear correlation coefficient is 0.73 (Fig. 2).

4.2. Sediment composition and water chemistry

The sediment consists of a sequence from organic-poor silty and sandy sediments going from the bottom of core PG2023 to ca. 4.5 m, followed by a transitional phase with a prevailing silt fraction and increasing organic carbon, gradually proceeding into brown organic gyttja which persists until the top of the core (core picture in Fig. 2). The lithology of core PG2022 is similar to that of core PG2023.

The average total carbon content of core PG2023 is 1 wt% below and 10.4 wt% above 4.7 m with maximum values of 14 wt% at 0.8 m

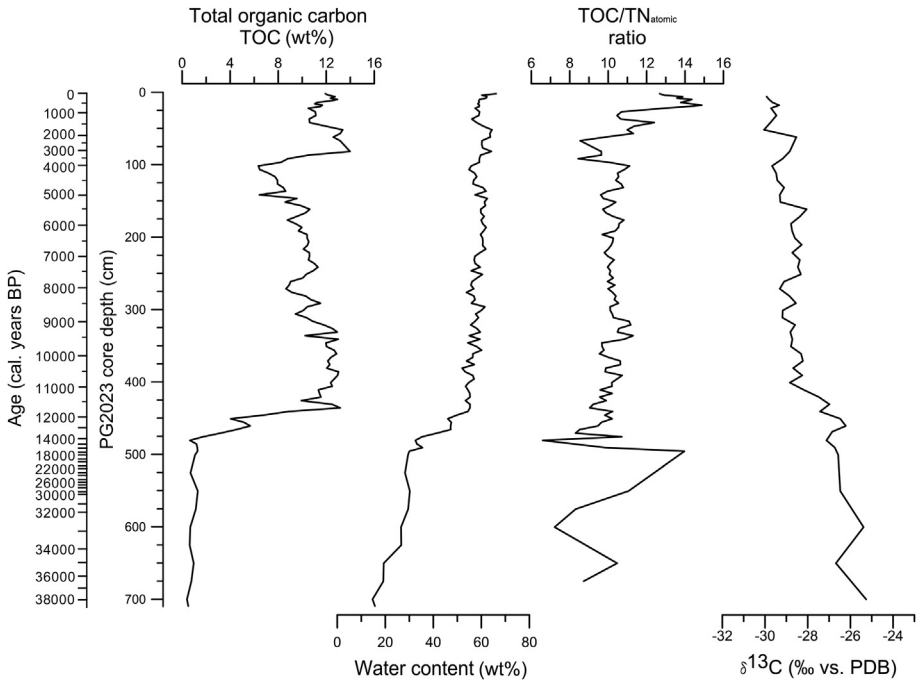

Fig. 3. Geochemistry of the organic fraction and the water content in sediment core PG2023.

(Fig. 3). TC and TOC differ by only 1.4 wt% on average, which is within the accuracy of measurements. The amount of inorganic carbon in the sediment is negligible because 1) TOC and TC correlate along the entire core, 2) XRD analyses revealed no carbonate, and 3) HCl treatment with samples showed no reaction. Therefore we consider TOC to be the exclusive carbon source. The TOC/TN_{atomic} ratio shows two peaks in the sandy lower part of core PG2023 reaching 10.5 and 14.0 at 6.5 m and 4.95 m, respectively. Between 4.5 and 0.95 m the TOC/TN_{atomic} ratio stays steadily at 10.3 on average, but is followed by strong fluctuations reaching a maximum value of 14.9 at 0.16 m core depth.

Below 4.5 m, $\delta^{13}C$ values are relatively high at −26.5‰ on average. Values above 4 m stay low at around −29‰ with minor fluctuations. The distinct peaks between ca. 1 and 0.5 m and, to lesser degree, at ca. 4.6 m core depth, correlate negatively with the TOC/TN_{atomic} ratio.

Only those elements discerned by XRF analysis that exhibit significant variations in the downcore elemental composition of PG2023 are mentioned in this paper (Fig. 4). The selection of elements was guided by the fact that the measurement validity for the lighter elements (e.g. Al and Si) is strongly reduced by the water content of the sediment during core scanning (Tjallingii et al., 2007). Therefore, our results are restricted to the heavier elements Sr, Zr, Rb and Br, given as counts per second (cps) or ratios. Findings from previous studies revealed Zr as an indicator of detrital minerogenic sediment input, Sr/Rb ratio as a grain-size indicator for the coarse (silt) fraction, and Br as an indicator of organic matter (Biskaborn et al., 2013b). Zr values are highest below 4.7 m, intermediate between 4.7 m and 1 m, and lowest in the uppermost 0.85 m. The Sr/Rb ratio is also high below 4.7 m with

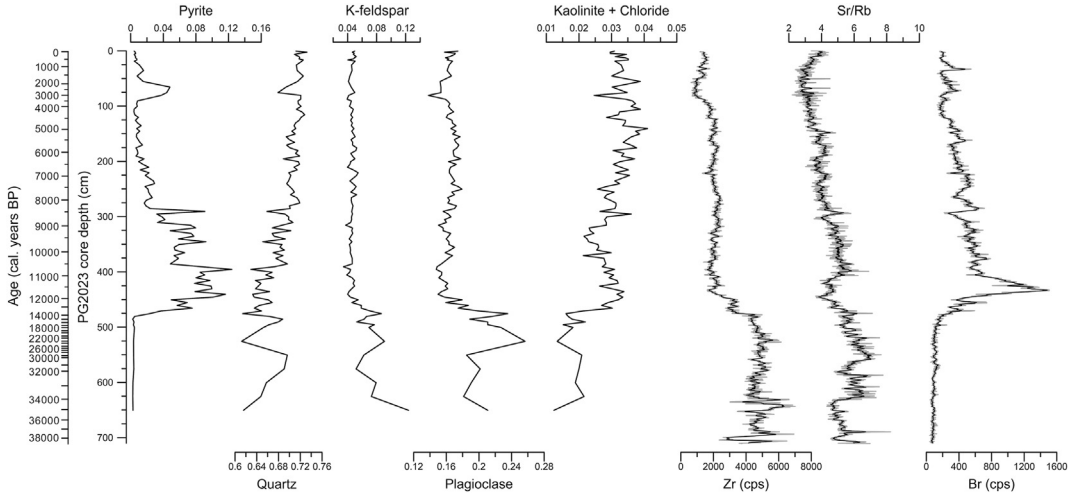

Fig. 4. Elemental and mineralogical sediment composition in the sediment core PG2023. Mineral contents were calculated as their ratio to the sum of the peak area intensity of the X-ray diffractometry data. X-ray fluorescence (XRF) scanner data are given as ratios or as counts per second (cps).

more intense fluctuations than Zr; it decreases somewhat steadily after partial recovery from a negative peak between 4.5 m and 4.1 m until it rises again in the uppermost 0.5 m. In core PG2023, Br correlates well with TOC, although the Br record shows notably higher values between 4.4 and 4.25 m than TOC whereas the Br peaks above 0.8 m are not as pronounced as the increases in TOC. Loss on ignition (LOI) values from core PG2022 vary between 18.1 and 47.5% and correlate well with TOC from PG2023, which is why LOI and TOC were used for tuning the age–depth model between the cores (Fig. 2).

The mineral composition from XRD analyses, plotted against the total intensities (Fig. 4), reveals distinct aggregation of framboidal pyrite between 4.8 m and 2.9 m in core PG2023 and a minor peak between 0.8 m and 0.6 m. Quartz shows the opposite trend to k-feldspar and plagioclase below ca. 4.7 m and steadily increases towards the top of the core, while both feldspars constantly decrease. Clay minerals, represented by kaolinite and chloride show low values below 4.7 m, intermediate values between 4.7 m and 3.2 m, and high values between 3.2 m and the top of the core.

Field measurements of lake-water pH varied between 7.3 and 8.3, before and after core retrieval, respectively. Noteworthy, the lake experienced heavy rainfall between the first sampling (including the depth profile) and the second sampling of the water surface. However, this does not explain the increase in pH of about one unit, because rainwater pH is usually slightly acidic. Thus we assume a methodical bias. Dissolved oxygen values have a maximum value of 9.5 mg L^{-1} at the surface and drop to a minimum of 8.6 mg L^{-1} at 250 cm water depth. Conductivity measurements revealed freshwater with only minor variations ranging from 27 to 29 µS cm^{-1} (Fig. 5).

4.3. Diatoms

Diatoms occur between 4.6 and 0 m depth in core PG2023. The diatom flora is composed of at least 201 taxa belonging to 44 genera. Principal taxa are shown in the species distribution diagram in Fig. 6. Selected minor diatom taxa having similar ecological preferences and displaying similar trends were combined in eco-taxonomic species complexes. The diatom assemblage is dominated by small benthic fragilarioid taxa, accounting for 63.1% of all diatoms present in all samples throughout the sediment core. Average percentages for the main species are *Staurosirella pinnata* (25.8%), *Staurosira venter* (form A 4.8%, form B 20.8%), *Staurosira construens* (4.1%), and *Staurosirella lapponica* (3.1%). Centric diatoms, such as *Aulacoseira* and *Cyclotella* are very scarce (<0.3%). Pennate planktonic taxa, such as *Tabellaria flocculosa*, are abundant (up to 26.1%) only in the uppermost 3 cm of the sediment succession.

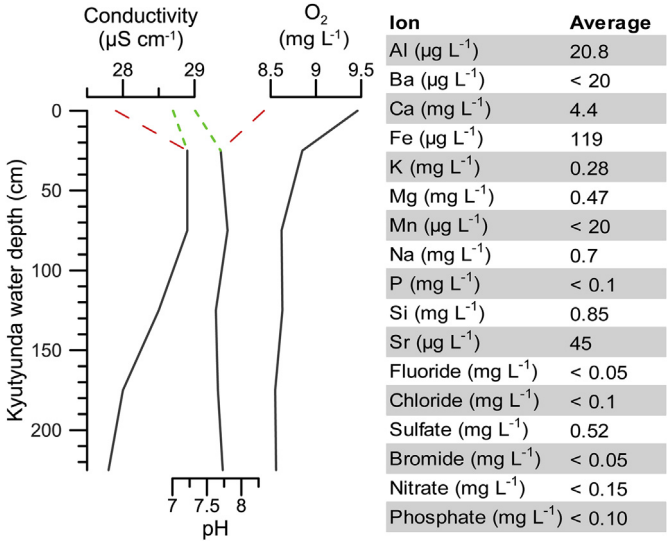

Ion	Average
Al (µg L^{-1})	20.8
Ba (µg L^{-1})	< 20
Ca (mg L^{-1})	4.4
Fe (µg L^{-1})	119
K (mg L^{-1})	0.28
Mg (mg L^{-1})	0.47
Mn (µg L^{-1})	< 20
Na (mg L^{-1})	0.7
P (mg L^{-1})	< 0.1
Si (mg L^{-1})	0.85
Sr (µg L^{-1})	45
Fluoride (mg L^{-1})	< 0.05
Chloride (mg L^{-1})	< 0.1
Sulfate (mg L^{-1})	0.52
Bromide (mg L^{-1})	< 0.05
Nitrate (mg L^{-1})	< 0.15
Phosphate (mg L^{-1})	< 0.10

Fig. 5. Water chemistry data of samples from Lake Kyutyunda at various water depths at core site PG2023, measured during field work in summer 2010. Dashed green lines lead to measurements of the surface water taken before coring; dashed red lines lead to measurements taken after core retrieval. Laboratory results of anions and cations measured in 2012 are given as average values in the table. (For interpretation of the references to colour in this figure legend, the reader is referred to the web version of this article.)

The CONISS cluster analysis on compositional diatom shifts combined with the broken-stick model produced three significant diatom zones. We further divided the uppermost zone following the next level of dissimilarity to emphasise the Anthropocene.

Benthic diatoms start to appear downcore at 4.6 m. Other samples from deeper parts of the core showed no evidence of diatom valves. Taxa appearing in the record at >5% abundance include *S. pinnata*, *Cymbella behrei*, *Cymbella diluviana*, *Gyrosigma attenuatum*-complex and *Amphora inariensis*-complex.

Diatom zone 1 (~12,100–8000 cal. years BP) begins with *Pseudostaurosira brevistriata*-complex dominant (max. 17.0%), which soon retreats, while other fragilarioids become more frequent and *Navicula jentzschii* appears at high abundances (max. 20.2%) between 4.2 m and 3.2 m. The sample resolution was increased to every 5 cm between 3 m and 2.8 m. In this section, a peak of *S. venter* form A is evident, while *N. jentzschii* is less frequent. Diatom valve concentrations are minimal when diatoms first appear and remain at their minimum values until 4.0 m (Fig. 7). They stay low throughout diatom zone 1 but show a subtle increase between 3.8 m and 3.6 m. Valve preservation, measured and calculated as the f-index (Ryves et al., 2001), is very poor in the lowest sample with sparse occurrences of diatoms. At 4.4 m, the f-index reaches its average level of ca. 0.8, and stays relatively constant throughout the sediment succession until the surface layers. The chrysophyte cyst/diatom (C/D) ratio reaches its maximum peak at 4.4 m and is, on average, slightly higher in the lower half than in the upper half of the sediment core. Reconstructed alkalinity (HCO_3^-) reaches its highest values of up to 48.9 mg L^{-1} at about 3.3 m and declines in the upper core section.

Diatom zone 2 (~8000–3300 cal. years BP) is characterised by high percentages of *S. venter* form B (max. 54.3%), but low average percentages of *S. venter* form A (2.0%), while other *Staurosira* taxa are not present or restricted to core depths below 2.0 m. At ca. 2.4 m *N. jentzschii* disappears and the abundance of naviculoid species starts to gradually increase. The diatom valve concentration increases slightly; valve preservation is generally very good but decreases towards the end of zone 2. The C/D ratio is at its lowest average values (6.5). In the middle of diatom zone 2, at 1.9 m, *S. venter* form A, *Staurosira subsalina*, and *S. lapponica* almost disappear, while *Navicula* spp. start to occur at higher abundances.

In diatom zone 3 (~3300–00 cal. years BP) the average abundance of *S. venter* form B decreases again, while *S. venter* form A starts to re-appear at frequencies similar to diatom zone 1. The most striking change in the diatom assemblage in this zone is the increase in epiphytic and benthic mono- and biraphid species, such as *Rossithidium pusillum*, *Achnanthidium minutissimum*-complex, *Karayevia laterostrata*, *Karayevia suchlandtii*, *Gomphonema*-complex, and *Navicula* spp. The diatom valve concentration in this zone suggests prominent changes and attains an extremely high maximum value of 6.4×10^8 diatom valves per gram dry sediment at 0.6 m. Diatom valve preservation is good with average values of 0.84 and the C/D ratio stays low: both show frequent but less extreme fluctuations.

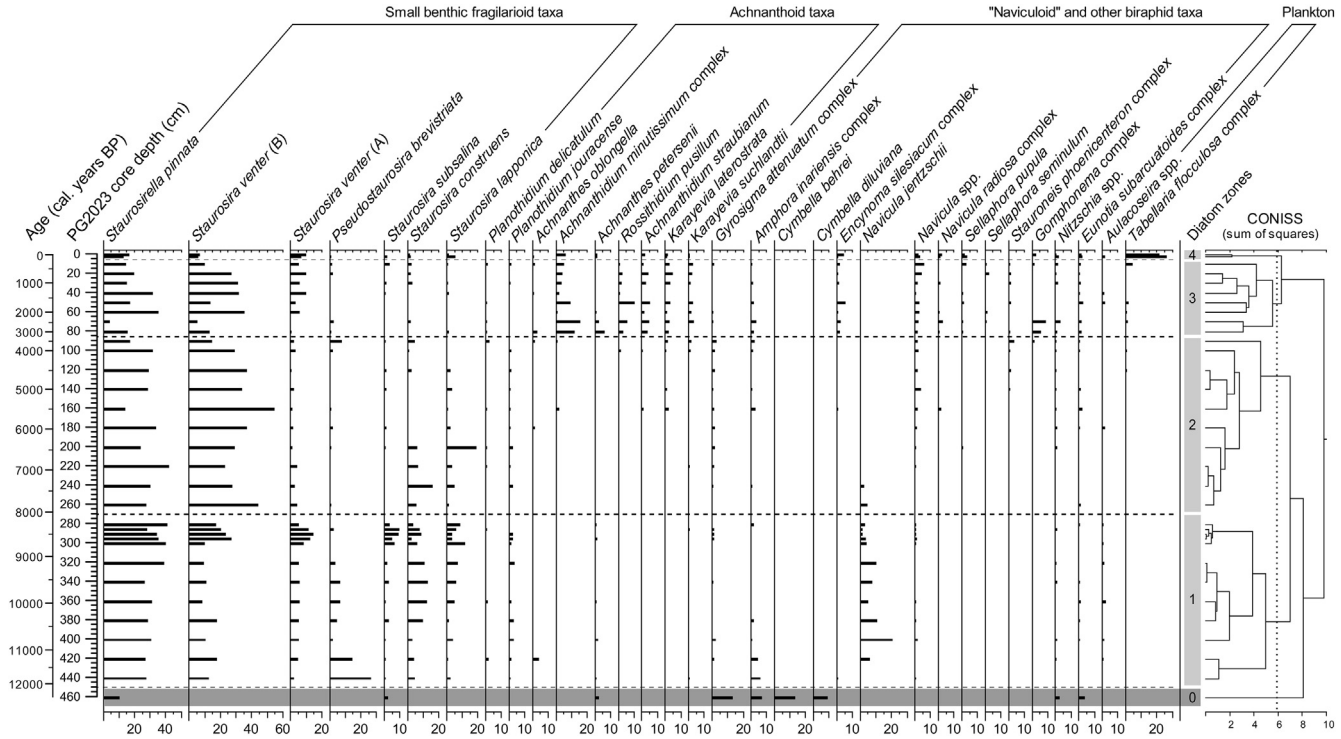

Fig. 6. Distribution of the relative abundances (%) of the most common diatom taxa in core PG2023 from Lake Kyutyunda, north-east Siberia. Diatom zones guided by a CONISS cluster analysis are delineated by dotted lines. The shaded area marks the sample at 4.6 m core depth with scarce diatom counts. Selected scarce diatom taxa were grouped into eco-taxonomic complexes. *Achnanthidium minutissimum*-complex: *A. minutissimum*, *A. affine*, *A. sacrophilum*. *Gyrosigma attenuatum*-complex: *G. attenuatum*, *G. acuminatum*, *G.* sp. *Amphora inariensis*-complex: *A. inariensis*, *A. indistincta*. *Encyonema silesiacum*-complex: *E. silesiacum*, *E. minutum*. *Navicula radiosa*-complex: *N. radiosa*, *N. cryptocephala*. *Stauroneis phoenicenteron*-complex: *S. phoenicenteron*, *S. anceps*, *Stauroneis gracilior*, *S. gracilis*. *Gomphonema*-complex: *G. clavatum*, *G. pseudoaugur*, *G. innocens*, *G. italicum*, *G. pala*, *G. parvulum*. *Eunotia subarcuatoides*-complex: *E. subarcuatoides*, *E. bilunaris*, *E. faba*, *E. soleirolli*, *E.* spp. *Tabellaria flocculosa*-complex: *T. flocculosa*, *T. fenestrata*.

Diatom zone 4 (last ~100 years), contains two samples between 3 cm and 0 cm and has low abundances of small benthic fragilarioid species with a prominent peak in the planktonic *T. flocculosa*-complex. Diatom valve concentrations decrease to values similar to core depths below 1 m. Valve preservation slightly decreases and the C/D ratio slightly increases.

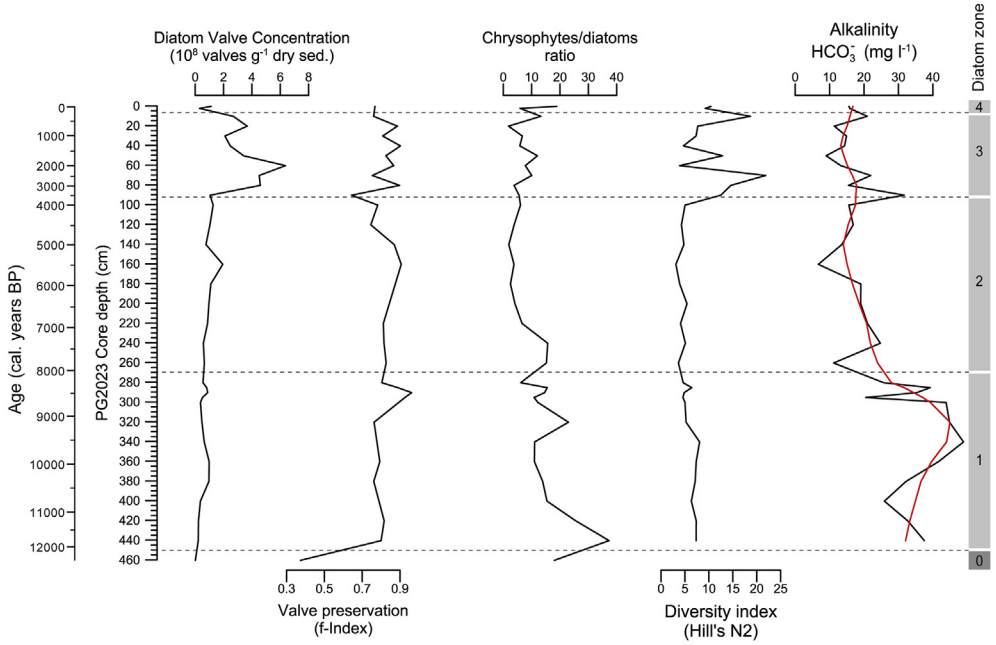

Fig. 7. Statistical results of the diatom valve concentration, preservation, diversity, chrysophyte cyst/diatom ratio, and diatom-inferred alkalinity, expressed as concentration of HCO_3^- ions in mg L^{-1}. Major alkalinity trends are summarised by a LOESS (locally estimated scatterplot smoothing, span: 0.25, red line). (For interpretation of the references to colour in this figure legend, the reader is referred to the web version of this article.)

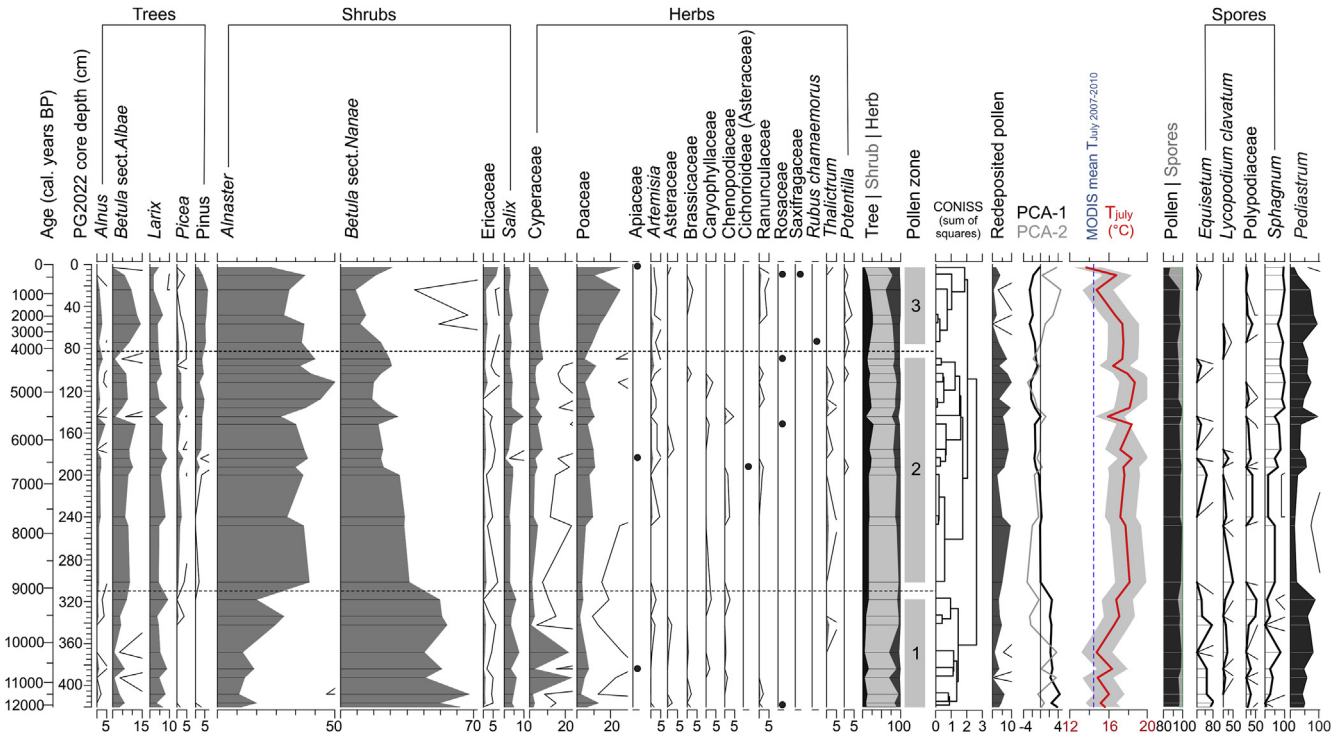

Fig. 8. Distribution of pollen and spores in core PG2022. Terrestrial pollen is given as the percentage of all terrestrial pollen counts and rare taxa are indicated by dots. Pollen zones are based on CONISS cluster analysis performed on terrestrial pollen taxa data. Re-deposited pollen is shown as percentages of the total pollen sum. Axes scores of the principal component analysis (PCA-1 and PCA-2) are shown, explaining 77% and 13%, respectively, of the total variance. The mean July temperature (T_{July}) reconstruction is based on the reduced WA transfer-function discussed in Klemm et al. (2016); dashed blue line is mean T_{July} from MODIS data for the period 2007–2010 AD. For comparison, the contribution of spores and pollen are given as percentages of their sum. Spore taxa percentages are based on the total spore sum. *Pediastrum* percentages are calculated from the total sum of pollen and non-pollen palynomorphs. (For interpretation of the references to colour in this figure legend, the reader is referred to the web version of this article.)

4.4. Pollen

The pollen assemblage comprises 27 terrestrial taxa. The pollen signal is dominated by shrub taxa of *Betula* sect. *Nanae* and *Alnaster*, which account for an average of 32.3% and 29.9%, respectively, over all core samples. Tree pollen of *Larix* and *Betula* sect. *Albae* have lower average values of 5.4% and 6.3%, respectively, which are similar to those of Cyperaceae and Poaceae pollen (5.5% and 8.9%, respectively). The CONISS cluster analysis distinguishes three pollen zones (Fig. 8). Pollen zone 1 (~11,200–9100 cal. years BP) is dominated by high shrub contributions of *Betula* sect. *Nanae* and *Salix*. Additionally, the samples with most Cyperaceae and *Equisetum* are located in this section. In pollen zone 2 (~9100–3600 cal. years BP), consistently high percentages of tree taxa are detected. This section also includes the highest values for redeposited pollen grains, and has the lowest *Pediastrum* percentages. Within pollen zone 3 (last 3600 years), herb pollen and Ericaceae shrub pollen contributions increase markedly. A high contribution of *Sphagnum* spores is seen in this uppermost section.

The first PCA-axis explains 77% of the total variance; high negative first axis scores are related to *Betula* sect. *Nanae* and positive scores are correlated with *Alnaster* and *Pinus*. On the second axis, which explains 13% of the variance within the dataset, a positive correlation with Cyperaceae and Poaceae is apparent.

The pollen-based climate reconstruction of T_{July} is weakly correlated to the first two PCA axes and shows a slight, but statistically significant correlation between the RDA-scores and the species optima ($p = 0.02$). The T_{July} estimate of the upper sample is 13.7 °C, which is close to the MODIS temperature for the region of 14.6 °C ($n = 11$) that provided the data for the climate transfer function. The relative T_{July} variation over the whole core reveals a variation of 5 °C. Cool July temperatures are inferred for the lowest samples dated to the beginning of the Holocene up till ~9900 cal. years BP and are followed by a gradual temperature increase. Warm July temperature is inferred for the early and especially mid Holocene from ~8900 to ~4500 cal. years BP. Two distinct short cold events were reconstructed at ~5500 and ~4500 cal. years BP, followed by a gradual cooling towards modern values.

5. Discussion

5.1. Late Pleistocene and the transition to the Holocene

The oldest part of the sedimentary record from Lake Kyutyunda is dated to ~38,000 cal. years BP. The pre-Holocene sediment succession consists of organic-poor siliciclastic sediments without diatoms and a dominant minerogenic sediment fraction with constantly high values of Zr, which is a common detrital indicator in Arctic regions (Bouchard et al., 2011). The negative correlation of feldspar (K-feldspar, plagioclase) with clay minerals (kaolinite and chlorite) corresponds with the Sr/Rb ratio, indicating that in siliciclastic sedimentary systems, Sr acts as a substitute for Ca in feldspar and Rb substitutes K in clay minerals. Hence, in core PG2023 the Sr/Rb ratio serves as a proxy for grain-size (Biskaborn et al., 2013b; Kalugin et al., 2007). Linear interpolation between the radiocarbon ages below 4.7 m depth (Fig. 2) indicates that the sediment accumulation rate during the late Pleistocene was much lower (~0.15 mm a^{-1}) than in the Holocene period (~0.4 mm a^{-1}), when organic matter started to accumulate in greater quantities (Fig. 3). Very low sedimentation rates of 0.05 mm a^{-1} between 4.7 and 5.6 m can be ascribed to shallow and variable basin morphology during this time causing an instable depositional

environment and possibly hiatuses in the pre-Holocene sediment succession due to erosional processes.

The isotopic composition of the organic fraction reveals constantly higher $\delta^{13}C$ values in the late Pleistocene than in the Holocene. Lake algae and most of the land plants belong to C3 plants, which preferentially use the lighter ^{12}C isotope during photosynthesis and they typically have $\delta^{13}C$ values of −25 to −30‰, while dissolved atmospheric CO_2 has values of about −7‰ (Kaufman et al., 2012; Meyers, 2003). The observed shift of the $\delta^{13}C$ values at the Pleistocene/Holocene boundary indicates a change in the catchment vegetation related to the major climate transition from dry and cold glacial conditions to generally wetter and warmer interglacial climate condition. Balascio and Bradley (2012) used decreasing $\delta^{13}C$ as a proxy for landscape stabilisation, which implies that soil development and establishment of denser vegetation could also have caused the decreasing $\delta^{13}C$ values in the Holocene sediments of Lake Kyutyunda.

During the late Pleistocene period, glaciation in the Verkhoyansk Mountain area was restricted to the western foreland of the Verkhoyansk Mountains, as evidenced by the small terminal moraines there (Stauch and Lehmkuhl, 2010). Prevailing coarse grain size, dominant detritic input, and lack of organic matter indicate high-energy sedimentary regimes with a lack of bioproduction. Thus we infer that the late Pleistocene environment around Lake Kyutyunda was cold and ice-free, supported by the presence of fluvial terraces and dunes in the study area, suggesting that it was not a lake at this time.

5.2. Early Holocene

The first diatom assemblage appeared at 12,400 cal. years BP with scarce and only poorly preserved valves of taxa, which in many cases are found only in this particular sample at 4.6 m core depth. This special diatom assemblage was dominated by benthic alkaliphilous *G. attenuatum*-complex together with *Cymbella* and *Staurosira* taxa, indicating a lack of clay habitats (Bennion, 1993) and suggestive of riverine activity. Riverine influence also promoted a high amount of allochthonous diatom valves in this section. Concomitant with a strong increase in clay minerals and a decrease in the detrital indicator Zr (Fig. 4), the diatom assemblage changed abruptly at about 11,800 cal. years BP in the early Holocene as a lake phase was established. This abrupt change in the downcore diatom distribution probably resulted from a rerouting of the Molodo River allowing the establishment of a depositional system during the Pleistocene–Holocene transition. As a consequence of increasing summer temperatures and hence increased thermokarst activity, the lake basin most likely originated as a cut-off from the main riverbed. The map in Fig. 2 shows meandering rivers and oxbow lakes near Lake Darkylach and Lake Kyutyunda supporting this supposition.

The diatom assemblage during the early Holocene was dominated by small fragilarioid species known to colonise benthic habitats during ice-covered periods in oligotrophic lakes (Biskaborn et al., 2012; Lotter and Bigler, 2000; Rudaya et al., 2009). Reconstructed alkalinity (HCO_3^-) reaches its highest values of up to 48.9 mg L^{-1} in the early Holocene (Fig. 7), reflected by the predominance of alkaliphilous and fragilarioid species such as *S. pinnata* (Lange-Bertalot et al., 2011).

Although the pollen/spores ratio remains relatively constant in the lower core sections, *Equisetum* spores accumulated at high quantities until ~9600 cal. years BP, correlating well with diatoms (e.g. *N. jentzschii*, *P. brevistriata*). A link between terrestrial and aquatic ecosystems through altered nutrient availability and catchment stability has been observed before, for example when *Alnus* emerged in the catchment (Bigler et al., 2006). Catchment changes could also have triggered shifts in the shoreline and littoral ecosystem represented by *Equisetum* stands associated with diatoms (Kairesalo, 1984) such as the periphytic diatom *N. jentzschii* (Heinsalu, 2000) and fragilarioid species.

The maximum peak in the chrysophyte cyst/diatom ratio at 11,800 cal. years BP (Fig. 7) is a result of nutritional strategies of "golden brown algae" producing resistant siliceous resting stages in cold and oligotrophic lakes (Smol, 1985). Although in Arctic regions periphytic chrysophyte taxa are abundant (Douglas and Smol, 1995), high C/D ratios may also reflect deeper waters and the interpretation remains conjectural. We observed a somewhat negative correlation between chrysophyte cysts and *Pediastrum*, a coenobial green algae favouring either shallow unstable conditions similar to ponds and marshes (Andreev et al., 2004; Bradbury et al., 1981) or nutrient enrichment and deeper water (Herzschuh et al., 2005; Zamaloa and Tell, 2005).

Starting at the bottom of core PG2022 at 12,100 cal. years BP, shrub pollen dominate (e.g. *Betula* sect. *Nanae*) while tree pollen is scarce (e.g. *Betula* sect. *Albae* and *Alnus*) or absent (e.g. *Picea* and *Pinus*). Thus, the earliest Holocene period is inferred to have a *open Larix forest* environment *similar to modern conditions* with cool mean T_{July} (14.7–16.4 °C, mean 15.5 °C) lasting until ~9900 cal. years BP. After a transitional phase of about a millennium, higher summer temperatures are inferred for between ~8900 and ~4500 cal. years BP ranging from 16.0 to 18.7 °C (mean 17.8 °C). High pollen percentages for *Alnus*, *Larix*, and *Picea* indicate a *more densely* forested catchment at Lake Kyutyunda.

Biskaborn et al. (2012) have shown that the occurrence of pyrite in lower core sections from north-eastern Siberian thermokarst lakes is linked to the formation of framboidal pyrites during prolonged seasonal lake-ice cover. The strong correlation between pyrite and TOC also implies that the formation of iron sulfide was linked to reduction of sulfates from organic matter under anoxic conditions (Rickard, 2012). In Lake Kyutyunda we found a distinct pyrite peak between ~13,500 and ~8900 cal. years BP and one subsequent peak at ~8400 cal. year BP, which may, when considering the 2-sigma error of 343 years in this core section, indicate the 8.2 cold event that is well described in Greenland ice-core studies (Thomas et al., 2007). This interpretation is also based on supportive evidence given by the peak accumulations of cold-adapted small benthic fragilarioid taxa such as *S. venter* form A and *S. subsalina* (Biskaborn et al., 2012; Lotter et al., 2010).

The transition from the early Holocene to the mid Holocene is characterised by relatively constant sedimentary conditions as indicated by the abiotic (Fig. 4) and biotic (Fig. 3) sediment properties. However, the transition between pollen zones 1 and 2 (~9000 cal. year BP) occurred a thousand years before the transition between diatom zones 1 and 2 (~8000 cal. year BP). This can either be interpreted as a delay in the interaction between the aquatic and terrestrial ecosystem development or a response to a driving force which affected only one of the two compared systems. We do not attach much importance to this lag because of the transitional character of this relatively small time period, and because the pollen-based reconstruction of July temperatures increases simultaneously with the major decrease in diatom-inferred alkalinity (Figs. 7 and 8). Shifts in alkalinity, however, have been explained by different processes. Given a large variety of lake and catchment settings, decreased alkalinity can either be related to (1) improved soil development and decreased mineral weathering leading to decreased base cation supply to the lake during enhanced catchment vegetation cover, which also provides increased organic acid influx (Laing et al., 1999; MacDonald et al., 2004; Paul et al., 2010; Rühland and Smol, 2005), (2) enhanced freshwater input (Tingstad et al., 2011), or (3) to lack of dense forests associated with decreased ion input into the lake water (Herzschuh et al., 2013). Our results

suggest that in the early Holocene, Lake Kyutyunda was situated in a tundra environment, where process (1) more likely determined the hydrochemistry of the lake, while process (3) was less relevant due to the minor impact of trees in the overall catchment setting.

The response of diatom species distributions to warming conditions is depicted generally by a decrease in small benthic fragilarioid taxa and an increase in naviculoid taxa at 6200 cal. years BP (Fig. 6). However, the different timing between pollen and diatom signals requires a more detailed investigation of the driving forces. In shallow boreal lakes with dominant benthic diatom communities, greater taxonomic diversity and increased growth of naviculoid taxa can be related to warm periods with a reduction in the duration of seasonal ice-cover (Bigler and Hall, 2003; Cherapanova et al., 2007; Douglas and Smol, 2010; Ford, 1990; Smol et al., 2005). We are aware that the terrestrial catchment setting can also influence the distribution of susceptible diatom species by changing water pH and nutrients, but the described dependence of diatoms to lake-ice cover has also been observed in Lake Sysy-Kyuele (Fig. 1), and verified by the occurrence of pyrite (Biskaborn et al., 2012).

5.3. Mid to late Holocene

Both diatom and pollen zones 3 start at ~4000 cal. years BP and show extreme increases in total organic carbon, *Pediastum*, and diatom diversity and valve concentrations. Intense fluctuations in the TOC/TN_{atomic} ratio and $\delta^{13}C$ values indicate fluctuating lake level and alternation in the relative inputs of lacustrine vs. terrestrial organic matter (Lenz et al., 2013).

Our results suggest that the late Holocene climate deterioration, as indicated by low pollen-inferred mean July temperatures and an establishment of a more open *Larix* forest, was accompanied by a major limnological regime shift that caused significant changes in the aquatic ecosystem. The regime shift in the catchment vegetation can be seen especially in the sharp increase of Poaceae pollen percentages and the lowest *Larix pollen* percentages below 2% in two samples of this section. However, the abrupt and essential improvement in growth conditions for a wider range of diatom taxa can be explained by substantial lake habitat changes. We hypothesise that Lake Kyutyunda became cut off from an important part of the local hydrographical system. As a consequence, the main source of organic carbon changed, as indicated by a drop in the TOC/TN_{atomic} ratio, followed by stepwise increases in the ratio as water depth decreased and macrophytes increased (Meyers and Teranes, 2002). Increased total organic carbon resulted not only because of enhanced bioproductivity but also from decreased dilution effects due to reduced input of minerogenic material (see Zr, Fig. 4). Reduced riverine input is also indicated by a decrease in redeposited pollen (Campbell, 1999) in pollen zone 3. As the depositional environment became calmer, a higher number of periphytic achnanthoid and naviculoid diatom taxa were able to inhabit the lake basin. Changes in the lake status during this time include improved nutrient availability, as reflected by increased diatom diversity and a decrease in the pollen/spores ratio associated with an increased nutrient supply from peat (Qualls and Richardson, 2003). A lack of turbulent hydrological conditions would prevent ventilation, and the increase in oxygen-consuming aquatic organisms and organic matter supply would explain the pyrite peak indicative of anoxic conditions near the water–sediment interface (Davison et al., 1985) between ~2000 and ~3000 cal. years BP.

The upper 3 cm of core PG2023 encompasses recent climate change. The sudden and striking increase of pennate diatoms such as *T. flocculosa*, a common acidophilous planktonic species in oligo- to mesotrophic shallow lakes (Lange-Bertalot et al., 2011; Paul et al., 2010), has been reported as a typical reaction of Artic shallow lake ecosystems to recent climate warming (Rühland et al., 2013, 2015; Smol et al., 2005). The distribution of *T. flocculosa* and other phytoplankton species in Scandinavia is significantly driven by rising water temperature (e.g. Hallstan et al., 2013). *T. flocculosa* is often recorded in the plankton forming zig-zag filaments and its increasing occurrence in the Andes was interpreted as a lengthening of the warm period and the duration and extent of thermal lake stratification (Michelutti et al., 2015). In very cold environments in Siberia, reduction of the length of the ice-covered period and hence extension of the duration of the growing season, is an important additional factor (Rühland et al., 2015). The simultaneous decreases in total diatom diversity and valve concentrations indicate a stressor to the ecosystem of shallow Arctic lakes, which are especially susceptible to the effects of climatic change in the Anthropocene (Smol and Douglas, 2007). However, pollen from core PG2022 shows no clear signal of recent warming, which can be attributed to either poor retrieval of the surface sediments (Russian peat coring technique) and/or the slow response of catchment forests to climate change (Herzschuh et al., 2013). The character and intensity of the recent aquatic ecosystem response can be attributed to increases in both summer and winter temperature, due to human impacts on the Earth's climate (IPCC, 2014).

5.4. Local ecosystem implications of annual climate dynamics

In palaeolimnological research, ecosystem dynamics in lakes and their catchments act as a filter between past climate forcings and the signal archived in the proxy record, such that (1) ecosystems that developed over long time scales tolerate disturbances without responding drastically until the disturbances exceed the resilience of the ecosystem (Zehe and Sivapalan, 2009); (2) aquatic ecosystems are more directly driven by terrestrial vegetation changes than by the thermal climate regime (Herzschuh et al., 2013); and (3) terrestrial indicators, such as pollen, provide information on mean summer temperatures, whereas aquatic organisms in boreal lakes strongly depend on the duration of lake ice (Lotter and Bigler, 2000).

Terrestrial and aquatic ecosystems in boreal environments are closely interlinked within a complex and dynamic natural system (Engstrom et al., 2000). However, prolonged seasonal lake-ice cover dampens diatom community responses to climate changes (Keatley et al., 2008) and hence decouples the aquatic and terrestrial ecosystems to a certain degree. The question arises whether winter temperature is the main driver of the seasonal length of lake ice. Reportedly, historical freeze and breakup dates of ice on lakes in the Northern Hemisphere reveal a shortening of the ice-covered period over a recording period of a few hundred years from before industrialisation until today (Magnuson et al., 2000; Robertson et al., 1992). Given that summer insolation decreased but winter insolation increased over the last millennia (Fig. 9), we suggest that winter temperature is the main natural factor influencing the length of seasonal lake-ice cover in Siberia during the Holocene.

Until now, the role of seasonality, which is especially pronounced in north-eastern Siberian climate records, has been underestimated in palaeoclimate reconstructions (Meyer et al., 2015). By using a terrestrial pollen-based reconstruction of mean July temperatures to infer summer climate trends and diatoms and authigenic pyrite as a winter signal (Fig. 9) we distinguish between summer and winter trends.

5.5. Conceptual integration in regional spatiotemporal palaeoclimate patterns

There is consensus that the Holocene Thermal Maximum (HTM)

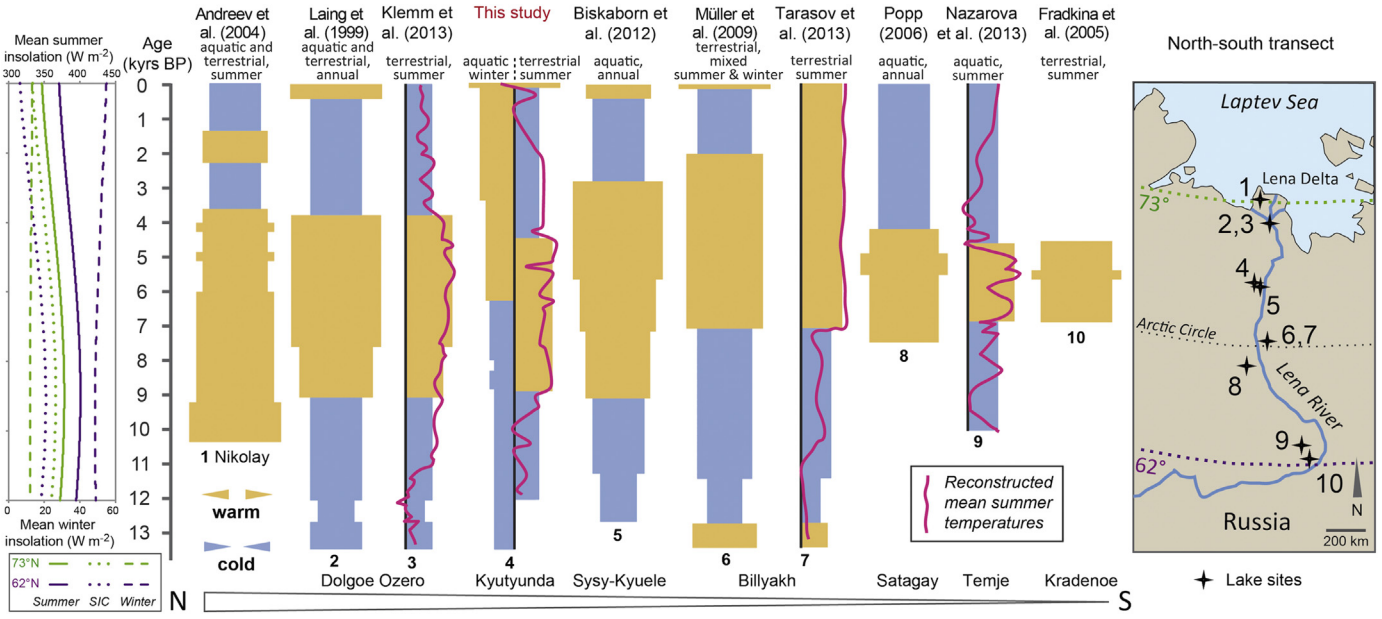

Fig. 9. Left: Holocene mean summer and winter insolation (90°–180° and 234° to −6° from vernal point, respectively) and the seasonal insolation contrast (SIC) in the study area along a latitudinal transect from Yakutsk to the northern Lena Delta. Data computed in Analyseries using the numerical solution of Earth's orbital parameters of Laskar et al. (2004). Middle: Spatiotemporal pattern of the Holocene Thermal Maximum in north-eastern Siberia, inferred from palaeolimnological climate reconstructions (Andreev et al., 2004; Biskaborn et al., 2012; Fradkina et al., 2005; Klemm et al., 2013; Laing et al., 1999; Müller et al., 2009; Nazarova et al., 2013; Popp, 2006; Tarasov et al., 2013) with the Lake Kyutyunda record. Type of indicators used and the season reconstructed is indicated. No differentiation between summer and winter is labelled as "annual". Right: Map of the ten palaeoclimate studies and latitudes used in the Holocene insolation graph. Climate curves of quantitatively reconstructed mean summer temperatures are indicated, if present.

in the Northern Hemisphere in the mid-Holocene is related to the higher maximum solar insolation (Bond et al., 2001; Miller et al., 2010a). However, this orbital forcing can be overprinted by secondary responses in the climate system. These processes are seen in the findings of Biskaborn et al. (2012) and the results of this study, which show that the onset of the HTM in north-eastern Siberia lagged by up to ~3000 years in southerly sites. According to global climate models (Renssen et al., 2012, 2009), this delay can be related to deglaciation processes of the Laurentide ice-sheet which brought cold air to parts of Siberia until ~7000 years BP. The ice-sheet theory of Renssen et al. (2009) serves well as an explanation of the delayed onset of the HTM, but the non-uniform ending of the warming has not previously been recognised.

In Fig. 9 we summarise the current knowledge about the HTM timing along a north–south transect in Siberia compiled from ten palaeolimnological studies at eight lakes. These studies used terrestrial and/or aquatic bioindicators together with abiotic sedimentological data, and show both a delayed onset and ending of the HTM along the latitudinal transect. At southerly sites, towards Central Siberia, the ending of the HTM is reportedly more difficult to detect. Assessment of palaeolimnological studies on the Holocene thermal development elsewhere in Russia supports this view (e.g. Anderson and Lozhkin, 2015; Andreev and Klimanov, 2000; Renssen et al., 2012; Salonen et al., 2011).

From a comparison of our findings to the known summer and winter insolation (Fig. 9), we suggest the following hypothetical scenarios as explanations of the delayed ending of the HTM in north-eastern Siberia. While summer insolation decreased over the Holocene, winter insolation increased, and seasonality — measured as the difference between summer and winter insolation (Seasonal Insolation Contrast, SIC, Fig. 9) — was higher in the early Holocene than today. Increasing continentality in Siberia, as a result of the large Eurasian land area, amplified the insolation-driven seasonal temperature difference, particularly in the south, causing extremely cold winters and large seasonal temperature differences in central Siberia during the early Holocene. Commonly used biotic and terrestrial climate indicators (proxies) depend on summer temperatures limiting their growth period. Our study shows that aquatic and abiotic sedimentary proxies also respond to winter climate conditions. The apparent lag in the ending of the central Siberian HTM may be ascribed to a step-wise exceedance of ecological thresholds in response to gradually increasing winter temperatures and decreasing seasonal insolation contrast. Given that strong contrasts between summer and winter temperatures in the Russian Arctic can lead to ambiguous indications of annual mean climate development (Meyer et al., 2015), we suggest that lake sediments from Siberia are better used for distinguishing between summer and winter temperature trends than for qualitatively inferring mean annual climate trends by using a combination of abiotic and biotic, terrestrial and aquatic proxies.

6. Conclusions

- Analyses of multiple biotic and abiotic proxies from radiocarbon-dated lake sediment cores reveal different climatic information over the Holocene in north-eastern Siberia, which is attributed to the varied responses of the proxies used to summer and winter forcings.
- Terrestrial pollen assemblages mainly reflect summer temperature development during the Holocene. A quantitative reconstruction revealed that a low mean T_{July} of 15.5 °C occurred until ~9900 cal. years BP and a high mean T_{July} of 17.8 °C occurred between ~8900 and ~4500 cal. years BP, followed by climate deterioration.
- In Siberian lakes, fragilarioid diatoms, compared to the whole diatom assemblage and sediment geochemistry, reflect at least partly winter climate conditions. At lake Kyutyunda, diatom species shifts, compared with the occurrence of framboidal pyrite, indicate prolonged seasonal lake-ice cover between ~13,500 and ~8900 cal. years BP and a subsequent isolated event

possibly reflecting the 8.2 ka cold event. A shorter period of winter lake-ice cover indicates increasing winter temperatures from the mid to late Holocene.

- A sudden increase of planktonic diatoms in response to both increased winter and summer temperatures represent a major change in the aquatic ecosystem, which may show that the natural insolation-driven climate development in Central Siberia is overprinted by human influence during the Anthropocene.
- Comparison between our findings and other palaeolimnological studies in north-eastern Siberia reveals the spatiotemporal pattern of the onset of the Holocene Thermal Maximum. Until the Laurentide ice-sheet vanished 7000 years ago, central Siberia was kept cold through the transport of cold air via the westerlies. However, the observed delay and probable uncertainty in the timing of the ending of the HTM may be a consequence of ecosystem resilience until the exceedance of ecological thresholds due to continued increasing winter temperatures and a decreasing contrast in seasonal insolation or because of a lack of differentiation between summer and winter trends in the palaeolimnological records.

Acknowledgements

Our study was financed by the Alfred Wegener Institute, Helmholtz Centre for Polar and Marine Research in Potsdam, Germany. Parts of our work were conducted in the laboratories of the Arctic and Antarctic Research Institute and the St. Petersburg State University of Russia. We thank Victor Strukov from the Radium Institute, St. Petersburg, for performing Pb-210 dating analysis, Julia Thom for helping with sample preparations for organic carbon analyses and Bastian Niemeyer for support with the Tilia software. We further thank Gerald Müller for his technical support and dedication in the helicopter expedition in 2010. All authors thank two anonymous reviewers for their careful reading and very good suggestions and comments.

Appendix A. Supplementary data

Supplementary data related to this article can be found at http://dx.doi.org/10.1016/j.quascirev.2015.08.014.

References

AMAP, 2012. Arctic Climate Issues 2011: Changes in Arctic Snow, Water, Ice and Permafrost. SWIPA 2011 Overview Report. Arctic Monitoring and Assessment Programme (AMAP), Oslo, 97 pp.

Anderson, P.M., Lozhkin, A.V., 2015. Late Quaternary vegetation of Chukotka (Northeast Russia), implications for Glacial and Holocene environments of Beringia. Quat. Sci. Rev. 107, 112–128.

Andreev, A., Tarasov, P., Schwamborn, G., Ilyashuk, B., Ilyashuk, E., Bobrov, A., Klimanov, V., Rachold, V., Hubberten, H.W., 2004. Holocene paleoenvironmental records from Nikolay Lake, Lena River Delta, Arctic Russia. Palaeogeogr. Palaeoclimatol. Palaeoecol. 209, 197–217.

Andreev, A.A., Klimanov, V.A., 2000. Quantitative Holocene climatic reconstruction from Arctic Russia. J. Paleolimnol. 24, 81–91.

Balascio, N., Bradley, R., 2012. Evaluating Holocene climate change in northern Norway using sediment records from two contrasting lake systems. J. Paleolimnol. 48, 259–273.

Battarbee, R.W., Jones, V.J., Flower, R.J., Cameron, N.G., Bennion, H., Carvalho, L., Juggins, S., 2001. Diatoms. In: Smol, J.P., Birks, H.J.B., Last, W.M. (Eds.), Tracking Environmental Change Using Lake Sediments. Kluwer Academic Publishers, Dordrecht, Netherlands, pp. 155–202.

Bennett, K.D., 1996. Determination of the number of zones in a biostratigraphical sequence. New Phytol. 132, 155–170.

Bennion, H., 1993. A Diatom-phosphorus Transfer Function for Eutropic Ponds in South-east England. University of London.

Berglund, B.E., Ralska-Jasiewiczowa, M., 1986. Pollen analysis and pollen diagrams. In: Berglund, B.E. (Ed.), Handbook of Holocene Palaeoecology and Palaeohydrology. Interscience, New York, pp. 455–484.

Bigler, C., Barnekow, L., Heinrichs, M.L., Hall, R.I., 2006. Holocene environmental history of Lake Vuolep Njakajaure (Abisko National Park, Northern Sweden) reconstructed using biological proxy indicators. Veg. Hist. Archaeobot. 15, 309–320.

Bigler, C., Hall, R.I., 2003. Diatoms as quantitative indicators of July temperature: a validation attempt at century-scale with meteorological data from northern Sweden. Palaeogeogr. Palaeoclimatol. Palaeoecol. 189, 147–160.

Biskaborn, B., Herzschuh, U., Bolshiyanov, D., Savelieva, L., Zibulski, R., Diekmann, B., 2013a. Late Holocene thermokarst variability inferred from diatoms in a lake sediment record from the Lena Delta, Siberian Arctic. J. Paleolimnol. 49, 155–170.

Biskaborn, B., Herzschuh, U., Bolshiyanov, D., Schwamborn, G., Diekmann, B., 2013b. Thermokarst processes and depositional events in a Tundra Lake, Northeastern Siberia. Permafr. Periglac. Process. 24, 160–174.

Biskaborn, B.K., Herzschuh, U., Bolshiyanov, D., Savelieva, L., Diekmann, B., 2012. Environmental variability in northeastern Siberia during the last similar to 13,300 yr inferred from lake diatoms and sediment-geochemical parameters. Palaeogeogr. Palaeoclimatol. Palaeoecol. 329, 22–36.

Boike, J., Wille, C., Abnizova, A., 2008. Climatology and summer energy and water balance of polygonal tundra in the Lena River Delta, Siberia. J. Geophys. Res. 113.

Bond, G., Kromer, B., Beer, J., Muscheler, R., Evans, M., Showers, W., Hoffmann, S., Lotti-Bond, R., Hajdas, I., Bonani, G., 2001. Persistent solar influence on north Atlantic climate during the Holocene. Science 294, 2130–2136.

Bouchard, F., Francus, P., Pienitz, R., Laurion, I., 2011. Sedimentology and geochemistry of thermokarst ponds in discontinuous permafrost, subarctic Quebec, Canada. J. Geophys. Res. Biogeosci. 116.

Bradbury, J.P., Leyden, B., Salgadolabouriau, M., Lewis, W.M., Schubert, C., Binford, M.W., Frey, D.G., Whitehead, D.R., Weibezahn, F.H., 1981. Late Quaternary environmental history of Lake Valencia, Venezuela. Science 214, 1299–1305.

Campbell, I.D., 1999. Quaternary pollen taphonomy: examples of differential redeposition and differential preservation. Palaeogeogr. Palaeoclimatol. Palaeoecol. 149, 245–256.

Cherapanova, M., Snyder, J., Brigham-Grette, J., 2007. Diatom stratigraphy of the last 250 ka at Lake El'gygytgyn, northeast Siberia. J. Paleolimnol. 37, 155–162.

Davison, W., Lishman, J.P., Hilton, J., 1985. Formation of pyrite in freshwater sediments: implications for CS ratios. Geochim. Cosmochim. Acta 49, 1615–1620.

Douglas, M.S.V., Smol, J.P., 1995. Paleolimnological significance of observed distribution patterns of chrysophyte cysts in arctic pond environments. J. Paleolimnol. 13, 79–83.

Douglas, M.S.V., Smol, J.P., 2010. Freshwater diatoms as indicators of environmental change in the High Arctic. In: Smol, J.P., Stoermer, E.F. (Eds.), The Diatoms: Application for the Environmental and Earth Sciences. Cambridge University Press, Cambridge, pp. 249–266.

Duguay, C., Soliman, A., Hachem, S., Saunders, W., 2012. Circumpolar and Regional Land Surface Temperature (LST) with Links to Geotiff Images and netCDF Files. Journal Volume, Pages. http://dx.doi.org/10.1594/PANGAEA.775962.

Engstrom, D.R., Fritz, S.C., Almendinger, J.E., Juggins, S., 2000. Chemical and biological trends during lake evolution in recently deglaciated terrain. Nature 408, 161–166.

Ford, M.S., 1990. A 10.000-yr history of natural ecosystem acidification. Ecol. Monogr. 60, 57–89.

Fradkina, A.F., Alekseev, M.N., Andreev, A.A., Klimanov, V.A., 2005. East Siberia (Based on data obtained mainly in Central Yakutia). In: Velichko, A.A., Nechaev, V.P. (Eds.), Cenozoic Climatic and Environmental Changes in Russia, Boulder, Colorado, pp. 89–103.

Grimm, E.C., 1987. Coniss - a Fortran-77 program for stratigraphically constrained cluster-analysis by the method of incremental sum of squares. Comput. Geosci. 13, 13–35.

Grove, J.M., 2004. Littles Ice Ages: Ancient and Modern. Routledge, New York.

Hallstan, S., Trigal, C., Johansson, K.S.L., Johnson, R.K., 2013. The impact of climate on the geographical distribution of phytoplankton species in boreal lakes. Oecologia 173, 1625–1638.

Heinsalu, A., 2000. Diatom stratigraphy and palaeoenvironment of the Yoldia Sea in northern Estonia. In: Proceedings of the Estonian Academy of Sciences, Geology. Estonian Academy Publishers, pp. 218–243.

Herzschuh, U., Pestryakova, L.A., Savelieva, L.A., Heinecke, L., Böhmer, T., Biskaborn, B., Andreev, A., Ramisch, A., Shinneman, A.L.C., Birks, H.J.B., 2013. Siberian larch forests and the ion content of thaw lakes form a geochemically functional entity. Nat. Commun. 4.

Herzschuh, U., Zhang, C.J., Mischke, S., Herzschuh, R., Mohammadi, F., Mingram, B., Kurschner, H., Riedel, F., 2005. A late Quaternary lake record from the Qilian Mountains (NW China): evolution of the primary production and the water depth reconstructed from macrofossil, pollen, biomarker, and isotope data. Glob. Planet. Change 46, 361–379.

Hijmans, R.J., Cameron, S.E., Parra, J.L., Jones, P.G., Jarvis, A., 2005. Very high resolution interpolated climate surfaces for global land areas. Int. J. Climatol. 25, 1965–1978.

IPCC, 2013. In: Stocker, T.F., Qin, D., Plattner, G.-K., Tignor, M., Allen, S.K., Boschung, J., Nauels, A., Xia, Y., Bex, V., Midgley, P.M. (Eds.), Climate Change 2013: the Physical Science basis. Contribution of Working Group I to the Fifth Assessment Report of the Intergovernmental Panel on Climate Change, p. 1535. Cambridge, United Kingdom and New York, NY, USA.

IPCC, 2014. In: Core Writing Team, Pachauri, R.K., Meyer, L.A. (Eds.), Climate Change 2014: Synthesis Report. Contribution of Working Groups I, II and III to the Fifth Assessment Report of the Intergovernmental Panel on Climate Change, p. 151. Geneva, Switzerland.

Jones, P.D., Briffa, K., Osborn, T., Lough, J., Van Ommen, T., Vinther, B., Luterbacher, J.,

Wahl, E., Zwiers, F., Mann, M., 2009. High-resolution palaeoclimatology of the last millennium: a review of current status and future prospects. Holocene 19, 3.
Jones, P.D., New, M., Parker, D.E., Martin, S., Rigor, I.G., 1999. Surface air temperature and its changes over the past 150 years. Rev. Geophys. 37, 173–199.
Juggins, S., 2014. Rioja: Analysis of Quaternary Science Data, R Package, 0.9.3 ed..
Juggins, S., 2007. C2 Version 1.5 User Guide. Software for Ecological and Palaeoecological Data Analysis and Visualisation. Newcastle University, Newcastle upon Tyne, UK, 73.
Kairesalo, T., 1984. The seasonal succession of epiphytic communities within an Equisetum fluviatile L stand in Lake Paajarvi, southern Finland. Int. Rev. Gesamten Hydrobiol. 69, 475–505.
Kalugin, I., Daryin, A., Smolyaninova, L., Andreev, A., Diekmann, B., Khlystov, O., 2007. 800-yr-long records of annual air temperature and precipitation over southern Siberia inferred from Teletskoye Lake sediments. Quat. Res. 67, 400–410.
Kaufman, D., Axford, Y., Anderson, R., Lamoureux, S., Schindler, D., Walker, I., Werner, A., 2012. A multi-proxy record of the Last Glacial Maximum and last 14,500 years of paleoenvironmental change at Lone Spruce Pond, southwestern Alaska. J. Paleolimnol. 48, 9–26.
Kaufman, D.S., Ager, T.A., Anderson, N.J., Anderson, P.M., Andrews, J.T., Bartlein, P.J., Brubaker, L.B., Coats, L.L., Cwynar, L.C., Duvall, M.L., Dyke, A.S., Edwards, M.E., Eisner, W.R., Gajewski, K., Geirsdottir, A., Hu, F.S., Jennings, A.E., Kaplan, M.R., Kerwin, M.N., Lozhkin, A.V., MacDonald, G.M., Miller, G.H., Mock, C.J., Oswald, W.W., Otto-Bliesner, B.L., Porinchu, D.F., Ruhland, K., Smol, J.P., Steig, E.J., Wolfe, B.B., 2004. Holocene thermal maximum in the western Arctic (0-180 degrees W). Quat. Sci. Rev. 23, 529–560.
Kaufman, D.S., Schneider, D.P., McKay, N.P., Ammann, C.M., Bradley, R.S., Briffa, K.R., Miller, G.H., Otto-Bliesner, B.L., Overpeck, J.T., Vinther, B.M., Arctic Lakes 2k Project, M., 2009. Recent warming reverses long-term arctic cooling. Science 325, 1236–1239.
Keatley, B.E., Douglas, M.S.V., Smol, J.P., 2008. Prolonged ice cover dampens diatom community responses to recent climatic change in High Arctic lakes. Arct. Antarct. Alp. Res. 40, 364–372.
Klemm, J., Herzschuh, U., Pestryakova, L.P., 2015. Vegetation, climate and lake changes over the last 7,000 years at the boreal treeline in northcentral Siberia. Quat. Sci. Rev. 147, 422–434.
Klemm, J., Herzschuh, U., Pisaric, M.F.J., Telford, R.J., Heim, B., Pestryakova, L.A., 2013. A pollen-climate transfer function from the tundra and taiga vegetation in Arctic Siberia and its applicability to a Holocene record. Palaeogeogr. Palaeoclimatol. Palaeoecol. 386, 702–713.
Kondratieva, K.A., 1989. Formation pattern of the cryolithozone morphology and thickness. In: Ershov, E.D. (Ed.), Geocryology of the USSR. Central Siberia. Nedra, Moscow.
Kotlyakov, V.M., Velichko, A.A., Vasil'ev, S.A., 2014. Moscow. In: Initial Human Colonization of Arctic in Changing Paleoenvironments, pp. 1–519.
Krammer, K., Lange-Bertalot, H., 1986–1991. Bacillariophyceae Band 2/2. Gustav Fischer Verlag, Stuttgart, pp. 1–4.
Kupriyanova, L.A., Alyoshina, L.A., 1972. Pollen and Spores of Plants from the Flora of European Part of USSR. Russian Academy of Science, Nauka, Leningrad, 1, 171 pp. (in Russian).
Kupriyanova, L.A., Alyoshina, L.A., 1978. Pollen and Spores of Plants from the Flora of European Part of USSR. Academy of Sciences USSR, Nauka, Leningrad, 184 pp. (in Russian).
Laing, T.E., Rühland, K.M., Smol, J.P., 1999. Past environmental and climatic changes related to tree-line shifts inferred from fossil diatoms from a lake near the Lena River Delta, Siberia. Holocene 9, 547–557.
Lange-Bertalot, H., Genkal, S.I., 1999. Diatomeen aus Sibirien I. Koeltz Scientific Books, 271.
Lange-Bertalot, H., Hofmann, G., Werum, M., 2011. Diatomeen im Süßwasser - Benthos von Mitteleuropa. Ganter Verlag, 908.
Lange-Bertalot, H., Metzeltin, D., 1996. Indicators of Oligotrophy. Koeltz Scientific Books, 390.
Laskar, J., Robutel, P., Joutel, F., Gastineau, M., Correia, A.C.M., Levrard, B., 2004. A long-term numerical solution for the insolation quantities of the Earth. Astron. Astrophys. 428, 261–285.
Lenz, J., Fritz, M., Schirrmeister, L., Lantuit, H., Wooller, M.J., Pollard, W.H., Wetterich, S., 2013. Periglacial landscape dynamics in the western Canadian Arctic: results from a thermokarst lake record on a push moraine (Herschel Island, Yukon Territory). Palaeogeogr. Palaeoclimatol. Palaeoecol. 381, 15–25.
Lotter, A.F., Bigler, C., 2000. Do diatoms in the Swiss Alps reflect the length of ice-cover? Aquat. Sci. 62, 125–141.
Lotter, A.F., Pienitz, R., Schmidt, R., 2010. Diatoms as indicators of environmental change in subarctic and alpine regions. In: Smol, J.P., Stoermer, E.F. (Eds.), The Diatoms: Application for the Environmental and Earth Sciences. Cambridge University Press, Cambridge.
MacDonald, G., Felzer, B., Finney, B.P., Forman, S., 2000. Holocene lake sediment records of Arctic hydrology. J. Paleolimnol. 24, 1–13.
MacDonald, G.M., Bennett, K.D., Jackson, S.T., Parducci, L., Smith, F.A., Smol, J.P., Willis, K.J., 2008. Impacts of climate change on species, populations and communities: palaeobiogeographical insights and frontiers. Prog. Phys. Geogr. 32, 139–172.
MacDonald, G.M., Edwards, T.W.D., Gervais, B., Laing, T.E., Pisaric, M.F.J., Porinchu, D.F., Snyder, J.A., Solovieva, N., Tarasov, P., Wolfe, B.B., 2004. Paleolimnological research from northern Russian Eurasia. In: Smol, J.P., Pienitz, R., Douglas, M.S.V. (Eds.), Long-term Environmental Change in Arctic and Antarctic Lakes. Springer Netherlands, pp. 349–380.
Magnuson, J.J., Robertson, D.M., Benson, B.J., Wynne, R.H., Livingstone, D.M., Arai, T., Assel, R.A., Barry, R.G., Card, V., Kuusisto, E., Granin, N.G., Prowse, T.D., Stewart, K.M., Vuglinski, V.S., 2000. Historical trends in lake and river ice cover in the Northern Hemisphere. Science 289, 1743–1746.
Matveev, I.A., 1989. Agricultural Atlas of the Yakut ASSR. GUGK, Moscow.
Meyer, H., Opel, T., Laepple, T., Dereviagin, A.Y., Hoffmann, K., Werner, M., 2015. Long-term winter warming trend in the Siberian Arctic during the mid- to late Holocene. Nat. Geosci. 8, 122–125.
Meyers, P.A., 2003. Applications of organic geochemistry to paleolimnological reconstructions: a summary of examples from the Laurentian Great Lakes. Org. Geochem. 34, 261–289.
Meyers, P.A., Teranes, J.L., 2002. Sediment organic matter. In: Last, W.M., Smol, J.P. (Eds.), Tracking Environmental Change Using Lake Sediments, Physical and Geochemical Methods, vol. 2. Kluwer Academic Publisher, Dordrecht, pp. 239–269.
Michelutti, N., Cooke, C.A., Hobbs, W.O., Smol, J.P., 2015. Climate-driven changes in lakes from the Peruvian Andes. J. Paleolimnol. 54, 153–160.
Miller, G.H., Alley, R.B., Brigham-Grette, J., Fitzpatrick, J.J., Polyak, L., Serreze, M.C., White, J.W.C., 2010a. Arctic amplification: can the past constrain the future? Quat. Sci. Rev. 29, 1779–1790.
Miller, G.H., Brigham-Grette, J., Alley, R.B., Anderson, L., Bauch, H.A., Douglas, M.S.V., Edwards, M.E., Elias, S.A., Finney, B.P., Fitzpatrick, J.J., Funder, S.V., Herbert, T.D., Hinzman, L.D., Kaufman, D.S., MacDonald, G.M., Polyak, L., Robock, A., Serreze, M.C., Smol, J.P., Spielhagen, R., White, J.W.C., Wolfe, A.P., Wolff, E.W., 2010b. Temperature and precipitation history of the Arctic. Quat. Sci. Rev. 29, 1679–1715.
Moore, P.D., Webb, J.A., Collison, M.E., 1991. Pollen Analysis. Blackwell Scientific Publications, Oxford.
Müller, S., Tarasov, P.E., Andreev, A.A., Diekmann, B., 2009. Late Glacial to Holocene environments in the present-day coldest region of the Northern Hemisphere inferred from a pollen record of Lake Billyakh, Verkhoyansk Mts, NE Siberia. Clim. Past 5, 73–84.
Müller, S., Tarasov, P.E., Andreev, A.A., Tütken, T., Gartz, S., Diekmann, B., 2010. Late Quaternary vegetation and environments in the Verkhoyansk Mountains region (NE Asia) reconstructed from a 50-kyr fossil pollen record from Lake Billyakh. Quat. Sci. Rev. 29, 2071–2086.
Nazarova, L., Luepfert, H., Subetto, D., Pestryakova, L., Diekmann, B., 2013. Holocene climate conditions in central Yakutia (Eastern Siberia) inferred from sediment composition and fossil chironomids of Lake Temje. Quat. Int. 290, 264–274.
PAGES 2k consortium, 2013. Continental-scale temperature variability during the past two millennia. Nat. Geosci. 6, 339–346.
Paillard, D., 1996. Macintosh program performs time-series analysis. Eos 77, 379.
Paul, C.A., Rühland, K.M., Smol, J.P., 2010. Diatom-inferred climatic and environmental changes over the last 9000 years from a low Arctic (Nunavut, Canada) tundra lake. Palaeogeogr. Palaeoclimatol. Palaeoecol. 291, 205–216.
Pestryakova, L.A., Herzschuh, U., Wetterich, S., Ulrich, M., 2012. Present-day variability and Holocene dynamics of permafrost-affected lakes in central Yakutia (Eastern Siberia) inferred from diatom records. Quat. Sci. Rev. 51, 56–70.
Pisaric, M.F.J., MacDonald, G.M., Velichko, A.A., Cwynar, L.C., 2001. The Lateglacial and Postglacial vegetation history of the northwestern limits of Beringia, based on pollen, stomate and tree stump evidence. Quat. Sci. Rev. 20, 235–245.
Popp, S., 2006. Late Quaternary Environment of Central Yakutia (NE Siberia): Signals in Frozen Ground and Terrestrial Sediments, Alfred Wegener Institute for Polar and Marine Research, Research Unit Potsdam (Unpublished PhD thesis). University Potsdam, p. 85.
Popp, S., Diekmann, B., Meyer, H., Siegert, C., Syromyatnikov, I., Hubberten, H.W., 2006. Palaeoclimate signals as inferred from stable-isotope composition of ground ice in the Verkhoyansk foreland, Central Yakutia. Permafr. Periglac. Process. 17, 119–132.
Porinchu, D.F., Cwynar, L.C., 2002. Late-Quaternary history of midge communities and climate from a tundra site near the lower Lena River, Northeast Siberia. J. Paleolimnol. 27, 59–69.
Prokopiev, V.S., Urzov, A.S., Budeleeva, S.S., Slastenov, Y.L., Yuganova, L.A., 1999. Geologic Map of Yakutia: the West Verkhoyansk Block, 1:500.000. Map Printing House of the Russian Geological Research Institute, St. Petersburg.
Qualls, R.G., Richardson, C.J., 2003. Factors controlling concentration, export, and decomposition of dissolved organic nutrients in the Everglades of Florida. Biogeochemistry 62, 197–229.
R Core Team, 2012. R: a Language and Environment for Statistical Computing. R Foundation for Statistical Computing, Vienna, Austria, ISBN 3-900051-07-0.
Ramsey, C.B., 2009. Bayesian analysis of radiocarbon dates. Radiocarbon 51, 337–360.
Reimer, P.J., Baillie, M.G.L., Bard, E., Bayliss, A., Beck, J.W., Blackwell, P.G., Ramsey, C.B., Buck, C.E., Burr, G.S., Edwards, R.L., Friedrich, M., Grootes, P.M., Guilderson, T.P., Hajdas, I., Heaton, T.J., Hogg, A.G., Hughen, K.A., Kaiser, K.F., Kromer, B., McCormac, F.G., Manning, S.W., Reimer, R.W., Richards, D.A., Southon, J.R., Talamo, S., Turney, C.S.M., van der Plicht, J., Weyhenmeye, C.E., 2009. IntCal09 and Marine09 radiocarbon age calibration curves, 0.50,000 years cal BP. Radiocarbon 51, 1111–1150.
Renssen, H., Seppä, H., Crosta, X., Goosse, H., Roche, D.M., 2012. Global characterization of the Holocene Thermal Maximum. Quat. Sci. Rev. 48, 7–19.
Renssen, H., Seppa, H., Heiri, O., Roche, D., Goosse, H., Fichefet, T., 2009. The spatial and temporal complexity of the Holocene thermal maximum. Nat. Geosci. 2,

410–413.
Rickard, D., 2012. Sulfidic Sediments and Sedimentary Rocks. Newnes, Elsevier, Amsterdam, 65, 816.
Robertson, D.M., Ragotzkie, R.A., Magnuson, J.J., 1992. Lake ice records used to detect historical and future climatic changes. Clim. Change 21, 407–427.
Rudaya, N., Tarasov, P., Dorofeyuk, N., Solovieva, N., Kalugin, I., Andreev, A., Daryin, A., Diekmann, B., Riedel, F., Tserendash, N., Wagner, M., 2009. Holocene environments and climate in the Mongolian Altai reconstructed from the Hoton-Nur pollen and diatom records: a step towards better understanding climate dynamics in Central Asia. Quat. Sci. Rev. 28, 540–554.
Rühland, K., Smol, J.P., 2005. Diatom shifts as evidence for recent Subarctic warming in a remote tundra lake, NWT, Canada. Palaeogeogr. Palaeoclimatol. Palaeoecol. 226, 1–16.
Rühland, K.M., Paterson, A.M., Keller, W., Michelutti, N., Smol, J.P., 2013. Global warming triggers the loss of a key Arctic refugium. Proc. R. Soc. Lond. B Biol. Sci. 280.
Rühland, K.M., Paterson, A.M., Smol, J.P., 2015. Lake diatom responses to warming: reviewing the evidence. J. Paleolimnol. 1–35.
Ryves, D., Juggins, S., Fritz, S., Battarbee, R., 2001. Experimental diatom dissolution and the quantification of microfossil preservation in sediments. Palaeogeogr. Palaeoclimatol. Palaeoecol. 172, 99–113.
Salonen, J.S., Seppä, H., Väliranta, M., Jones, V.J., Self, A., Heikkilä, M., Kultti, S., Yang, H., 2011. The Holocene thermal maximum and late-Holocene cooling in the tundra of NE European Russia. Quat. Res. 75, 501–511.
Savelieva, L.A., Raschke, E.A., Titova, D.V., 2013. Photographic Atlas of Plants and Pollen of the Lena River Delta. St. Petersburg State University, St. Petersburg, 114.
Shahgedanova, M., 2002. Climate at present and in the historical past. In: Shahgedanova, M. (Ed.), The Physical Geography of Northern Eurasia. Oxford University Press, Oxford, pp. 70–102.
Simpson, G.L., Oksanen, J., Simpson, M.G.L., 2014. Package 'Analogue'.
Smol, J.P., 1985. The ratio of diatom frustules to chrysophycean statospores: a useful paleolimnological index. Hydrobiologia 123, 199–208.
Smol, J.P., Douglas, M.S.V., 2007. Crossing the final ecological threshold in high Arctic ponds. Proc. Natl. Acad. Sci. U. S. A. 104, 12395–12397.
Smol, J.P., Wolfe, A.P., Birks, H.J.B., Douglas, M.S.V., Jones, V.J., Korhola, A., Pienitz, R., Rühland, K., Sorvari, S., Antoniades, D., Brooks, S.J., Fallu, M.A., Hughes, M., Keatley, B.E., Laing, T.E., Michelutti, N., Nazarova, L., Nyman, M., Paterson, A.M., Perren, B., Quinlan, R., Rautio, M., Saulnier-Talbot, E., Siitoneni, S., Solovieva, N., Weckstrom, J., 2005. Climate-driven regime shifts in the biological communities of arctic lakes. Proc. Natl. Acad. Sci. U. S. A. 102, 4397–4402.
Stauch, G., Lehmkuhl, F., 2010. Quaternary glaciations in the Verkhoyansk Mountains, Northeast Siberia. Quat. Res. 74, 145–155.
Sundqvist, H.S., Kaufman, D.S., McKay, N.P., Balascio, N.L., Briner, J.P., Cwynar, L.C., Sejrup, H.P., Seppa, H., Subetto, D.A., Andrews, J.T., Axford, Y., Bakke, J., Birks, H.J.B., Brooks, S.J., de Vernal, A., Jennings, A.E., Ljungqvist, F.C., Ruehland, K.M., Saenger, C., Smol, J.P., Viau, A.E., 2014. Arctic Holocene proxy climate database - new approaches to assessing geochronological accuracy and encoding climate variables. Clim. Past 10, 1605–1631.
Tarasov, P.E., Mueller, S., Zech, M., Andreeva, D., Diekmann, B., Leipe, C., 2013. Last glacial vegetation reconstructions in the extreme-continental eastern Asia: potentials of pollen and n-alkane biomarker analyses. Quat. Int. 290, 253–263.
Telford, R.J., 2015. palaeoSig: Significance Tests of Quantitative Palaeoenvironmental Reconstructions. R package, 1.1.3 ed.
Telford, R.J., Birks, H.J.B., 2011. A novel method for assessing the statistical significance of quantitative reconstructions inferred from biotic assemblages. Quat. Sci. Rev. 30, 1272–1278.
Thomas, E.R., Wolff, E.W., Mulvaney, R., Steffensen, J.P., Johnsen, S.J., Arrowsmith, C., White, J.W.C., Vaughn, B., Popp, T., 2007. The 8.2 ka event from Greenland ice cores. Quat. Sci. Rev. 26, 70–81.
Tingstad, A.H., Moser, K.A., MacDonald, G.M., Munroe, J.S., 2011. A similar to 13,000-year paleolimnological record from the Uinta Mountains, Utah, inferred from diatoms and loss-on-ignition analysis. Quat. Int. 235, 48–56.
Tishkov, A., 2002. Boreal forests. In: Shahgedanova, M. (Ed.), The Physical Geography of Northern Eurasia. Oxford University Press, Oxford, pp. 217–233.
Tjallingii, R., Rohl, U., Kolling, M., Bickert, T., 2007. Influence of the water content on X-ray fluorescence core-scanning measurements in soft marine sediments. Geochem. Geophys. Geosyst. 8.
Vysotsky, B.P., 1970. Geological Map of the USSR, 1:200 000. Series Nizhnelenskaya. Sheet R-51-XXI, XXII. Nedra, Moscow.
Wanner, H., Beer, J., Butikofer, J., Crowley, T.J., Cubasch, U., Fluckiger, J., Goosse, H., Grosjean, M., Joos, F., Kaplan, J.O., Kuttel, M., Muller, S.A., Prentice, I.C., Solomina, O., Stocker, T.F., Tarasov, P., Wagner, M., Widmann, M., 2008. Mid- to Late Holocene climate change: an overview. Quat. Sci. Rev. 27, 1791–1828.
Wanner, H., Solomina, O., Grosjean, M., Ritz, S.P., Jetel, M., 2011. Structure and origin of Holocene cold events. Quat. Sci. Rev. 30, 3109–3123.
Zamaloa, M.D., Tell, G., 2005. The fossil record of freshwater micro-algae Pediastrum meyen (Chlorophyceae) in southern South America. J. Paleolimnol. 34, 433–444.
Zehe, E., Sivapalan, M., 2009. Threshold behaviour in hydrological systems as (human) geo-ecosystems: manifestations, controls, implications. Hydrol. Earth Syst. Sci. 13, 1273–1297.